Dynamics of Layer Growth in Protein Crystallization

Peter G. Vekilov[†] and J. Iwan D. Alexander*[,‡]

Department of Chemistry and Center for Microgravity and Materials Research, University of Alabama—Huntsville, RI Building D-29, Huntsville, Alabama 35899, and Department of Mechanical and Aerospace Engineering and National Center for Microgravity Research on Fluids and Combustion, Glennan 416, Case Western Reserve University, Cleveland, Ohio 44106-7222

Received July 29, 1999

Contents

I. Introduction

Proteins are the elementary building units for all living creatures and are essential components for information and energy processing in living systems. The need to understand genome structure−function correlations for this group of natural compounds has emerged as a focus of intense recent investigations.[1] Although advances in nuclear magnetic resonance techniques continue to increase the upper limit to the size of protein molecules that can be studied by this method,[2] the diffraction of X-rays, electrons, or neutrons is the most widely used method for protein structure investigations. To resolve atoms that are, typically, 1.5−2 Å apart, these diffraction methods require single crystals that are as large as several tenths of a millimeter in all three dimensions and have low defect contents and high compositional and structural uniformity. Recent advances in protein expression, characterization, and purification techniques, as well as beam and detector technology and in computational crystallography, have greatly accelerated the rate at which protein structures can be solved.[3] However, the preparation of diffraction-quality crystals has emerged as the bottleneck in the route toward macromolecular crystal structure determinations.[4,5]

Beyond protein single-crystal growth, progress in various biochemical and biomedical research and production tasks is impeded by lack of insight into protein nucleation and growth mechanisms. For instance, the slow dissolution rate of protein crystals is used to achieve sustained release of medications, such as insulin.[6−10] Work on the crystallization of other proteins that can be dispensed in a similar manner (e.g., interferon-α and human growth hormone) is currently underway. If the administered dose consists of a few, larger, equidimensional crystallites, steady medication release rates can be maintained for longer periods than for doses comprised of many smaller crystallites. To achieve such

[†] University of Alabama—Huntsville. Phone: 256-890-6892. Fax: 256-890-6944. E-mail: peter@cmmr.uah.edu.
[‡] Case Western Reserve University. Phone: 216-368-6045. Fax: 216-368-6445. E-mail: ida2@po.cwru.edu.

10.1021/cr9800558 CCC: $35.00
Published on Web 05/18/2000

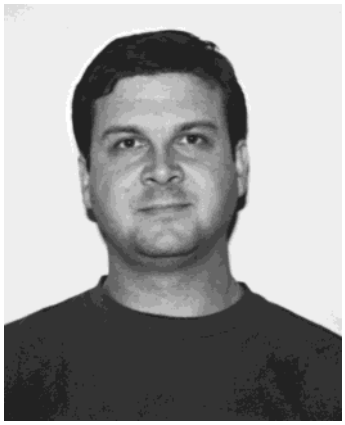

Peter Vekilov was born in Sofia, Bulgaria, in 1963. He received his M.S. degree with Honors in Chemistry in 1985 from Moscow State University and his Ph.D. degree in 1991 from the Russian Academy of Sciences, Institute of Crystallography, under the supervision of Professor Dr. Alexander A. Chernov. After postdoctoral stints in Bulgaria and Japan, he worked as a Research Scientist at the Center for Microgravity and Materials Research (CMMR) at the University of Alabama in Huntsville, AL, with Professor Franz Rosenberger. Since 1998 he has been an Assistant Professor of Chemistry at the same University and led the Physics and Chemistry of Crystallization Group at the CMMR. In 1995 he received the Young Scientist Award of the International Union of Crystallography for research in protein crystallization. His main focus is protein crystallization and other related phase transitions and their biomedical implications. Unsteady kinetics, instabilities, and defect formation in protein and inorganic crystals are prime foci of scientific effort.

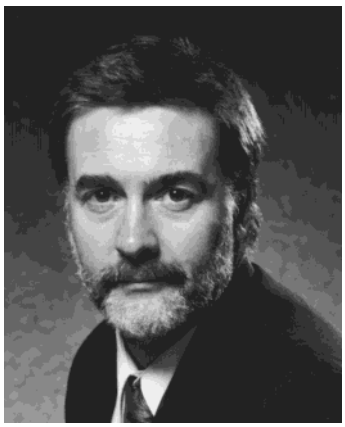

Iwan Alexander was born in Cardiff, Wales, in 1955. He received his B.Sc. in Geology and Oceanography from the University College Swansea in 1977 and his Ph.D. degree from Washington State University in 1981. Between 1982 and 1985 he was a postdoctoral researcher with Robert F. Sekerka in the Departments of Physics and Mathematics at Carnegie-Mellon University in Pittsburgh, PA. In late 1985 he moved to NASA's Marshall Space Flight Center as a visiting scientist and in 1987 joined the Center for Microgravity and Materials Research at the University of Alabama in Huntsville, AL, as a Senior Research Scientist. He later became Associate Director of the center and an Associate Professor of Physics. Since 1998 he has been an Associate Professor of Mechanical and Aerospace Engineering at Case Western Reserve University and the Chief Scientist for fluids at the National Center for Microgravity Research on Fluids and Combustion. His recent research has involved the investigation of heat, mass, and momentum transfer processes in terrestrial and space-based fluid and solid–liquid phase change systems and on the interaction between macroscopic transport and interfacial processes.

size distributions, crystal nucleation times must be short so that all crystals grow at the same decreasing supersaturation.

Other biomedical applications include situations where pathological conditions are related to the formation of crystals or other ordered solid aggregates in the human body. An often cited example is the crystallization of hemoglobin C and the polymerization of hemoglobin S that cause, respectively, the CC and sickle cell diseases.[11−13] Crystallization of the proteins in the eye retina underlies the pathology of cataract formation.[14]

Aside from their obvious medical and biotechnical significance, another, often unrecognized, application of protein crystallization is its use as a model for crystallization phenomena that occur in a variety of systems.[15] Thus, they are potentially useful to scientists from a number of different disciplines. Examples include water freezing in clouds and oceans,[16] solidification in the Earth's interior,[17] the pulling of 12 and 18 in. semiconductor boules,[18] etc. Given the resolution limits of modern surface characterization techniques, proteins are particularly attractive for studies of fundamental crystal growth mechanisms. For example, the size of the protein molecules (a few nanometers) and the typical time scales for growth (a few seconds between sequential discrete growth events) are within reach of the current advanced experiment techniques. On the other hand, the molecular masses typical of most protein molecules still leave thermal equilibration times relatively short. Thus, conclusions drawn from studies of protein model systems may still be meaningful for small molecule crystallization. In this regard, proteins could be a better model than, for instance, colloidal crystals.[19−21]

The above factors led to the emergence of macromolecular crystallization as a distinct area of research in the early 1980s. Since then, the field has benefited from concepts and methods developed in other research areas. For instance, the application of direct light scattering and other methods used to probe colloids led to quantitative measurements of molecular interactions and crystal nucleation in protein solutions (see refs 22−26 and references therein). Fluid dynamics analyses were applied to characterize the convective-diffusive supply fields in the solutions from which the crystals grow. Explanations of the differences between terrestrially grown protein crystals and those grown in microgravity,[27−29] have largely been based on such analyses. Interferometric and scanning probe techniques, first used by inorganic crystal growers[30,31] and surface scientists, provided insight into growth processes on a near-molecular level.[32−39] A variety of methods to establish and maintain advantageous supersaturation, temperature, and solution composition conditions have helped to achieve reproducible improved perfection of protein crystals.[8,40,41]

In this paper, we review recent results that explain some morphological and kinetics phenomena that occur during layer-wise growth of protein crystals. The explanations are based on ideas arising from the field of "nonlinear dynamics". For the crystal growth processes that are the main themes of this review, "dynamics" refers to unsteady collective behavior and bunching of molecular steps on growth surfaces. These dynamics arise due to the interactions between individual growth steps (crystal layer edges) moving on the crystal−solution interface. "Kinetics", on the

other hand, refers to the forces responsible for individual growth step motion and the underlying mechanisms through which molecules are incorporated into potential growth sites at these steps. Such a distinction is to a large extent limited since there is a clear interdependence between step dynamics and kinetics.

A significant fraction of the studies of protein growth dynamics were performed using the protein lysozyme, most often extracted from hen egg white. This enzyme hydrolyzes polysaccharides in bacterial cell walls[42] and was one of the first proteins studied by X-ray diffraction.[43−45] It is still widely used in studies of protein folding dynamics[46] and is particularly attractive for crystal growth research because its thermophysical properties are well characterized and because it was used in numerous prior studies (for a review, see ref 25). Numerous recent crystallization mechanism studies, see below, using a wide range of other proteins have validated the results obtained with this material and justified lysozyme as a useful model system for growth studies, see sections II and III below.

Quantitative and qualitative results drawn from the small number of protein systems studied in detail show that there is a strong correspondence between the growth behavior and mechanisms of these protein crystals with data and theories accumulated over some 70 years of research into the crystallization of inorganic small-molecule crystals. Thus, while for some yet-to-be studied protein systems there may indeed turn out to be significant fundamental departures from existing crystal growth theories, there is no quantitative experimental evidence for this at this time.

This review deliberately omits several areas of recent research related to protein crystallization. Protein molecular interactions in solutions have been discussed in a series of papers (see refs 47 and 48). Results on nucleation of protein crystals are summarized in ref 26. For a general theoretical introduction to the problem, see refs 49 and 50. Two-dimensional crystallization of proteins is referenced in refs 51−53. For treatises on protein crystallization techniques, see the available or forthcoming editions of refs 54 and 55. A comprehensive list of references on impurity effects is provided in ref 56 and on precipitants and solubility in ref 57. Our discussion will not consider the possibility of conformational heterogeneity and flexibility of the protein molecular structure,[54,55] which may be important for the perfection and utility of certain protein crystals. The reason for this is that current characterization techniques lack the submolecular resolution needed for the in-situ evaluation of conformational effects.

Section II begins with a discussion of the generation of new crystal growth layers. It is shown that if the crystals approach the sizes needed for their applications (typically >100 μm), growth layers are generated at a few preferred locations. The layers then spread to cover the entire face. This leads to long trains of almost parallel steps that exhibit step bunching and other unsteady behavior that results in undesirable defects. Examples of possible crystal defects produced by such unsteady growth behavior are provided in section III. In section IV we show that growth is unsteady and results in compositional and structural nonuniformities. The causes of this unsteadiness are discussed in terms of macroscopic nonequilibrium thermodynamics concepts. The microscopic mechanisms of the instability are discussed in section V, and possible means of controlling or suppressing them are reviewed in section VI. In section VII we discuss the role of impurities in unsteady growth processes and, in particular, the effects of enhanced impurity supply to the interface. From here we develop, in section VIII, recommendations for variations in the transport conditions that will provide growth conditions that will allow undesirable unsteady growth behavior. Depending on the protein in question, desirable conditions may require the reduced-gravity environment of space or may need a forced flow of the nutrient solution. Finally, in section IX it is seen that step bunching can affect step propagation velocities. Future research directions in this field are considered in section X.

II. Step Generation and Propagation

Crystals grow by ordered addition of growth units to a nucleation center. This requires suitable sites at which growth units can attach and conform to the crystal structure. Ideally, these growth sites are molecular configurations at the growth interface that provide an incoming molecule with exactly one-half of the neighbors of a molecule in the crystal bulk and were called half-crystal positions or kinks.[58−60] For growth above the roughening transition temperature, such half-crystal positions (or kink sites) are abundant even at equilibrium.[61] The frequency with which molecules are incorporated into the crystal structure depends only on the impingement frequency and the attachment activation energy. For such rough surfaces, the crystal's growth rate and shape are controlled by the transport processes responsible for delivering growth material to the interface or heat away from the interface. Growth under these conditions is referred to as normal growth. This is the growth mode of most melt-grown crystals (for example, bulk semiconductors and oxide crystals used for microprocessors and optoelectronic device technologies; for further reading, see refs 62 and 63.

For crystal surfaces below the roughening transition temperature, the bond energy between two molecules in the crystal (proportional to the enthalpy of crystallization or to the surface energy) is higher than the thermal energy of a molecule[61] and the crystal is faceted. At equilibrium, the kink or growth sites can only be located at the edges of unfinished crystal planes on the surface. Indeed, at room temperature, thermal fluctuations have been suggested to result in abundant half-crystal positions at the unfinished layer edges. These are called growth steps or just steps.[64,70] For inorganic crystals, the emergence of such growth steps is associated with 2D or surface nucleation of new layers[65−68] or dislocations cropping out on the face.[69−71] However, due to the small sizes of inorganic molecules and the considerably faster kinetics, direct evidence of many of the

growth mechanisms have not been obtained prior to the advances in protein crystallization reviewed below.

A. Step (Growth Layer) Generation

1. Dislocations, 2D Nucleation, and Crystallites

Most protein crystals display well-defined facets, and it has been confirmed at the microscopic level that growth occurs via the spreading of layers from growth step sources such as dislocations and 2D nucleation. Ex-situ electron microscopy observations have resolved individual growth steps on (101) and (110) facets of tetragonal lysozyme.[72] In-situ atomic force microscopy[73−75] has produced particularly instructive images of growth step generation at screw dislocation outcrops, see Figure 1, and of 2D-nucleation-induced islands, see Figure 2.

Most recent AFM observations on a larger number of other proteins and viruses[37,38,76−80] have reproduced the whole body of growth morphology and kinetics scenarios suggested for inorganic growth. These include layer spreading from dislocations and 2D nuclei, annihilation of growth steps coming from different sources at the face, and impediment of step propagation by foreign particles. When a foreign particle or a newly formed crystallite lands on the growing crystal surface, it may orient in register with the underlying lattice. In this case, it serves as a prolific source of new growth layers, see Figure 3, until the height of the adjacent crystal surface rises above it and engulfs it. Misaligned microcrystals and particles may also be incorporated into the crystal.

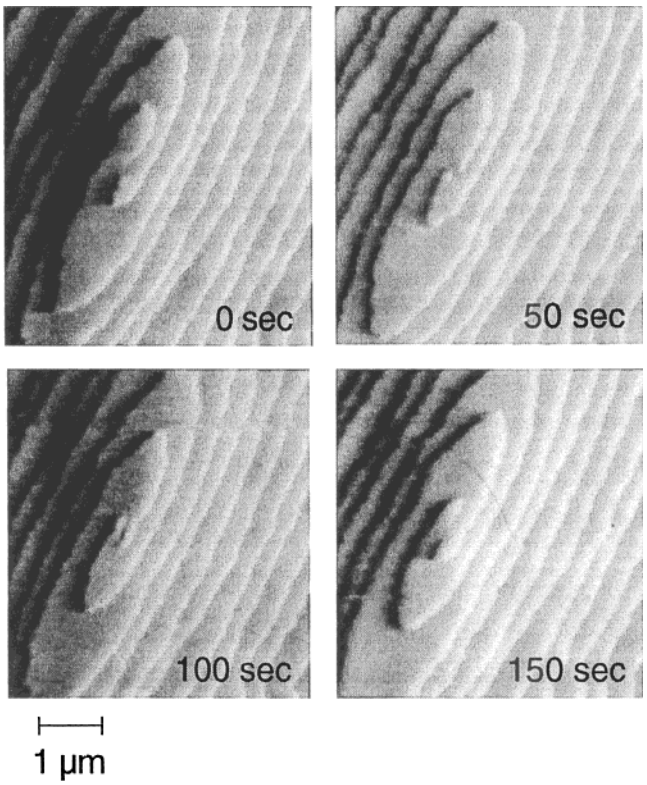

Figure 1. Spiral step source at outcrop of screw dislocation on a (110) face of lysozyme. Sequence of atomic force microscopy micrographs. (Adapted with permission from ref 74).

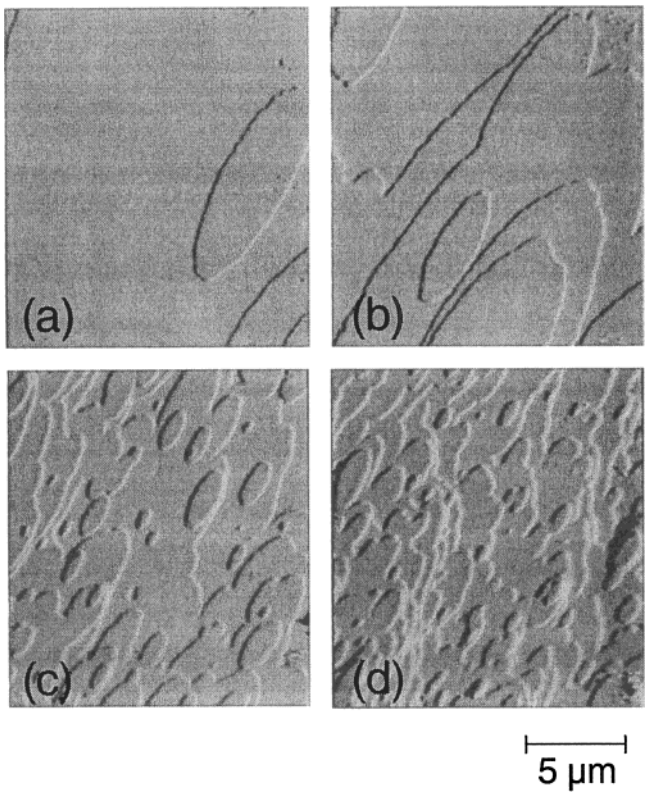

Figure 2. 2D nucleation-induced islands on a (110) face of tetragonal lysozyme. Island density increases with supersaturation from a to d. (Adapted with permission from ref 73).

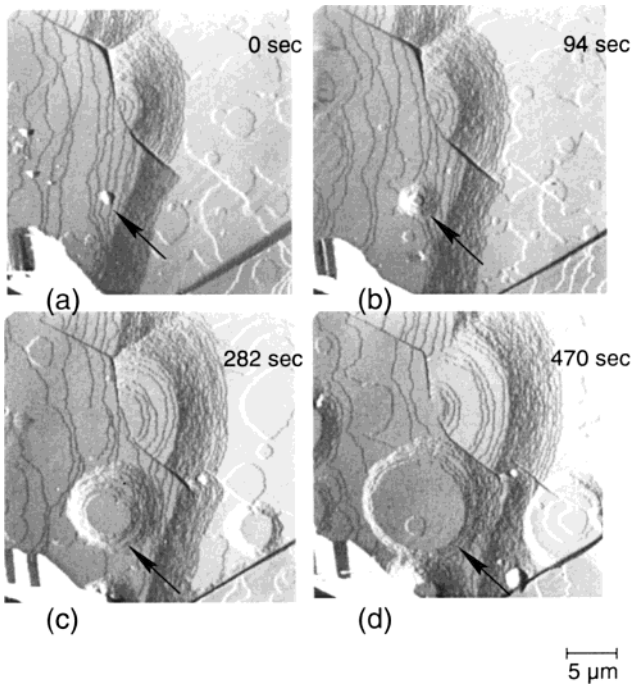

Figure 3. Series of AFM images showing the landing of microcrystal (indicated by arrows) on the surface of a (111) face of a growing cubic crystal of satellite tobacco mosaic virus. This microcrystal serves as a source of growth layers. It grows in thickness significantly slower than the large crystal, presumably due to the low probability of 2D nucleation on its small top surface. This will eventually result in engulfment. Such events provide the major source of growth layers during the growth of these virus crystals. (Adapted with permission from ref 79).

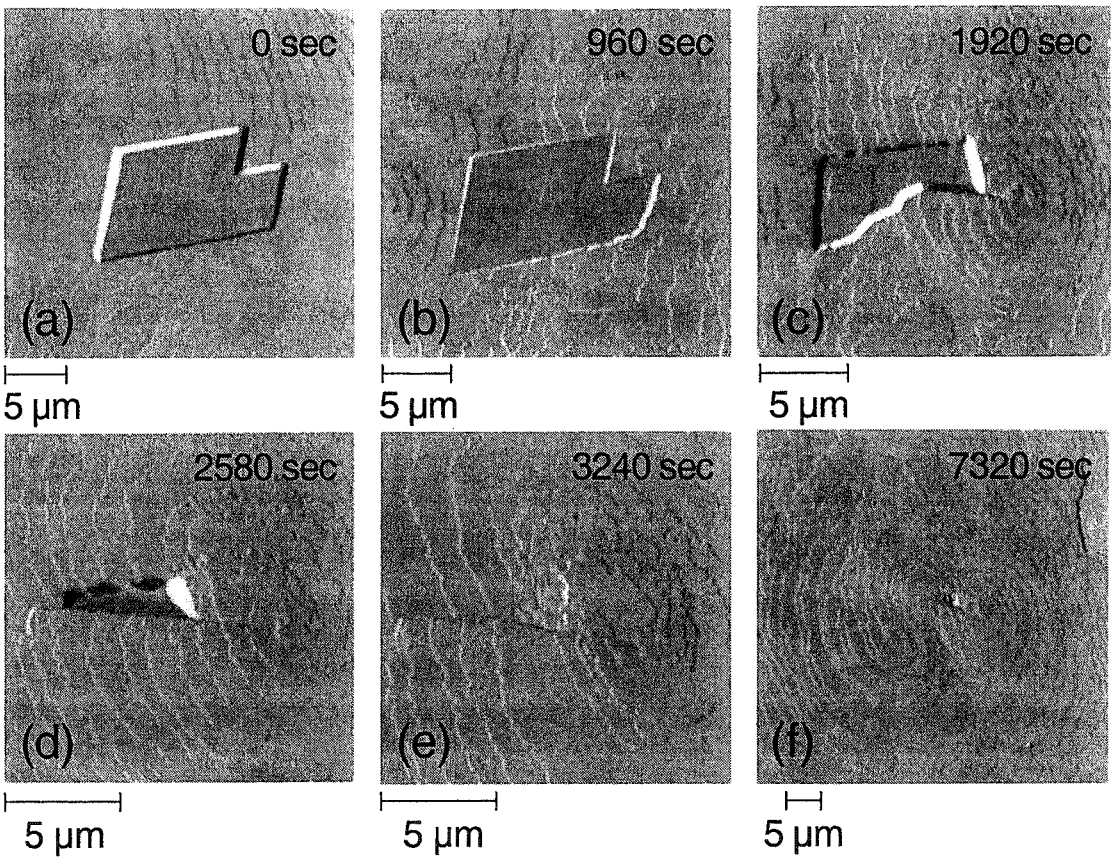

Figure 4. Series of AFM images showing the incorporation of a microcrystal 15 μm × 8 μm into a larger growing crystal of the protein canavalin. A lattice mismatch clearly exists between the two crystals. As the small crystal is consumed by the larger one, a planar defect and a bundle of screw dislocations form and propagate into the larger crystal. (Adapted with permission from ref 76).

Either case can result in the creation of dislocation bundles that operate as a strong source of growth layers, Figure 4.

There has been only one report[79] of normal growth of a protein: apoferritin, the hollow shell of the iron-transport protein ferritin,[81] Figure 5a. In previous quasielastic light scattering studies, it was found that apoferritin has a low surface energy. Despite the low surface energy, its rough surface morphology seems incompatible with the good faceting typically observed with both apoferritin and ferritin crystals.[82] This contradiction was resolved by recent studies that reveal that this protein grows by layer generation (exclusively by 2D nucleation) and spreading, Figure 5b.[83] Thus, earlier observations may be attributed to a high content, up to ~50% of the dry protein mass, of protein inhomogeneities in the used material[84] or to the high thermodynamic driving force used in ref 79 that may have caused a kinetic phase transition to a rough growth interface.[85,86]

2. Localization of 2D Nucleation: Bulk-Transport Nonuniformities and Defect Pinning

Interferometric studies of the evolution of growth morphologies of lysozyme provided the first evidence for localization of 2D nucleation.[25,32−34,87] While inferior in spatial resolution to AFM, interferometry is nonintrusive and permits the study of microscopic morphologies across entire macroscopic facets. This makes it possible to correlate bulk-transport-induced compositional inhomogeneities and the response of the crystal morphology. A high-resolution interferometric approach (200 Å depth resolution, image acquisition times ~3 s) was developed specifically for protein crystallization studies.[34] The method uses one face of a growing protein crystal as one of the interferometer mirrors. Spatial and temporal information about the surface relief is extracted by digitizing the interferometric intensity and its time variations. In this way, information about the growth step source activity is obtained by monitoring the facet slope p (proportional to step density) in the neighborhood of step generators. The time history of the tangential step velocity v is also recorded since changes in v reflect changes in the mechanism of growth unit incorporation.

Figure 6 shows the development of the morphology of a (101) face as a function of crystal size and supersaturation $\sigma = \ln(C/C_{eq})$, C and C_{eq} being the actual and the equilibrium protein concentrations.[87] For the small crystal (Figure 6a), growth did not start until $\sigma > 1.3$ and the flat face was preserved as the crystal grew. Hence, it was concluded that growth steps were generated by randomly distributed 2D nucleation, in agreement with earlier observations on lysozyme using electron microscopy and AFM, see section II.A.1 and refs 72−75. With increasing supersaturation/growth rate and facet size, layer generation preferentially occurred along the crystal edges. The specific nucleation sites moved with time,

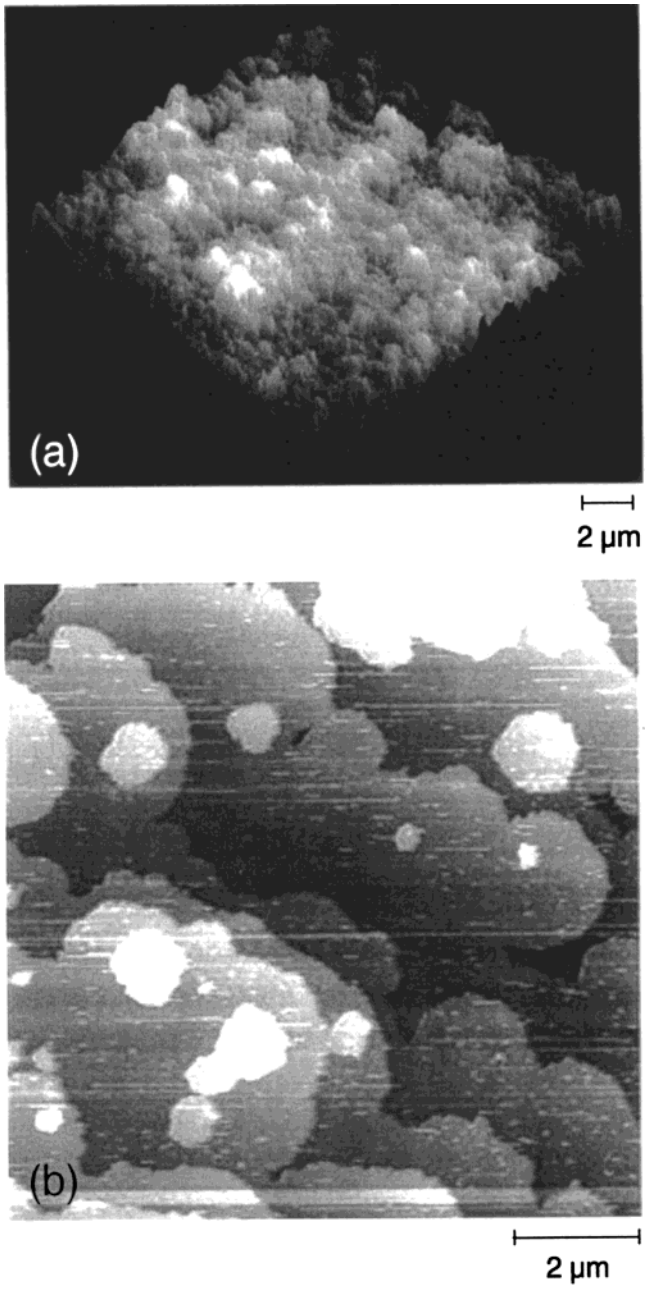

Figure 5. AFM visualization of interfacial morphology during growth of a (111) face of cubic apoferritin crystals: (a) rough surface (Adapted with permission from ref 79); (b) smooth facet growing by 2D layer generation and spreading.

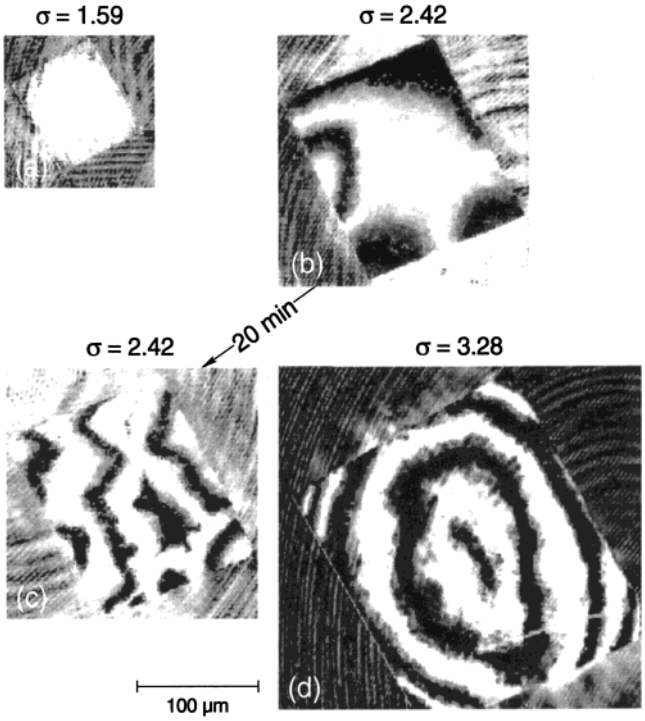

Figure 6. Development of growth morphology on a (101) HEWL face with crystal size and supersaturation, in the absence of an active dislocation step source. Interferometric visualization of growth morphology. In this method, the crystal face of interest is used as one of the mirrors of a two-beam interferometer. Thus, if the crystal is aligned so that the singular crystal planes are perpendicular to the incident beam, the interferograms represent topographic maps of the interface. Time elapsed between b and c is 20 min. Supersaturation indicated for each frame. (Reprinted with permission from ref 87. Copyright 1996.)

compare part b and c of Figure 6. With further increases of facet size and supersaturation σ, the steps were predominantly generated at the facet corners rather than at facet centers (see Figure 6d). This trend was observed in numerous experiments on {101} and {110} faces. This change in location of the nucleation sites can be explained by an increase in the nonuniformity of solute supply from the bulk nutrient as the crystal size and growth rate increase.[88−91] This leads to higher interfacial supersaturation (and, thus, a higher probability of nucleation) closer to the crystal's edges. Recently, using atomic force microscopy, the same transition from random to edge-localized 2D nucleation was found for ferritin and apoferritin crystals.[83] Since the diffusivity of the large ferritin molecules is significantly lower than that of lysozyme, the characteristic transport length is greater and the transition between the two modes occurs at sizes of about 200 μm.

In a few observations, however, steps persistently originated at locations near corners or edges, even at small crystal sizes or low growth rates; see, e.g., the frame sequence of Figure 4 in ref 92. Yet, these crystals did not grow at $\sigma \leq 1.6$. Thus, apparently no active dislocation step sources were present, and the pinning of the step generation locations was probably due to other lattice defects[93−95] that can locally enhance 2D nucleation.[95−98]

Thus, it appears that localized generation of new growth layers is quite common in protein crystallization, especially when crystal sizes reach those needed for X-ray structure determinations. This leads to long trains of quasiparallel steps propagating along the interface. Parallel step trains such as this are prone to unsteadiness that results in defects. This will be discussed below in sections IV−VI.

3. Evolution of the Dislocation Sources of Growth Layers

As above, this evolution was studied using interferometry.[87] The crystal face, shown in Figure 7, was initially free of screw dislocation step sources. At smaller crystal size and growth rate, the surface was flat, indicating growth by uniformly distributed 2D nuclei, Figure 7a. The higher growth rate and su-

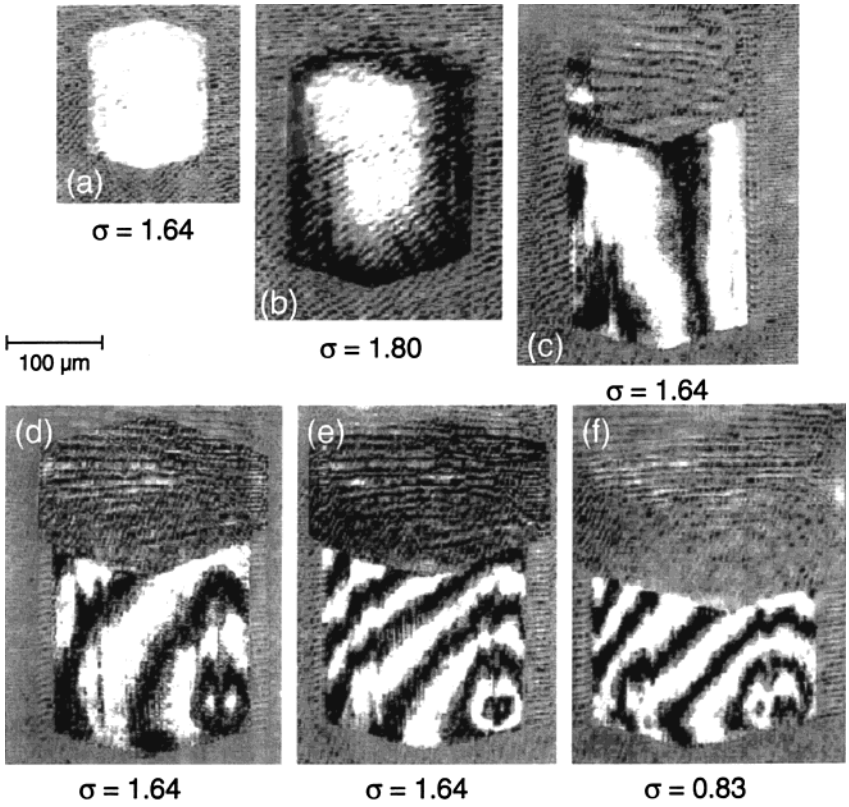

Figure 7. Interferometric monitoring of the growth morphology on a (110) face of a lysozyme crystal. Between b and c the supersaturation was temporarily increased to 2.84 and 3.22 (see text). This results in the dislocation step sources seen in c−f. (Reprinted with permission from ref 87. Copyright 1996 Elsevier Science.)

persaturation σ, in Figure 7b caused nucleation along the facet edges to dominate. The temperature was then lowered in steps to obtain supersaturation levels of $\sigma = 2.84$ and subsequently $\sigma = 3.22$. After a few hours, T was increased to 20 °C ($\sigma = 1.64$). The facet morphology remained essentially identical to Figure 7b. The only effect of these sharp supersaturation changes was the appearance of a second crystal on top of the first one. No interference fringes appeared on its top face. This means that the new crystal was substantially misoriented with respect to the first one. This explains why no steps originated from the reentrant angle between the two crystals, in contrast to Figure 3 in section II.A.1. The new crystal grew much more rapidly than the first one, even at low σ's, as can be seen from their relative change in lateral dimensions in Figure 7c−f.

After overnight growth at $\sigma = 1.64$, a hillock was observed at the lower left part of the facet of the first crystal, Figure 7c. This hillock persisted for about a day, in which the studied face grew about 13 μm. Hence, the hillock was most likely formed by dislocation outcrops at this location. Then steeper hillocks (visible in Figure 7d) supplied steps that eventually covered the facet. The supersaturation was kept constant for several hours, during which the top face grew by about 4 μm and the growth hillock became much steeper, Figure 7e**.** After further growth at $\sigma = 0.83$, the hillock slope increased further, Figure 7f, despite the lower supersaturation. Upon further decrease to $\sigma = 0.55$, the hillock slope remained practically unchanged.

The continuing (and apparently anomalous) increase of the hillock slope at constant or decreasing σ can be explained as follows. The dislocation groups active in Figure 7c−f have probably formed in response to the drastic temperature decreases or supersaturation increases. The response is most likely manifested through the trapping of a foreign particle or a drop of nutrient liquid.[99] Since initially no growth activity resulted, the dislocation group must have had a net Burgers vector (vector sum of the vectors of lattice mismatch comprising each dislocation in the group[100]) of zero and a large circumference.[64,101,102] Closely packed dislocations tend to diverge during growth since this decreases the elastic energy of the group.[103] When the distance between any pair of neighboring dislocations reaches about 10 critical 2D-nucleus radii,[64,104,105] one (or more) dislocation group(s) will start generating growth steps, provided that it has a smaller circumference and larger net Burgers vector. Furthermore, as the dislocations continue to fan out, their activity will increase. If several of the secondary (or tertiary) dislocation bunches attain growth activity, they will compete and interact.

Observations of long-term changes and short-term variations in the activity of the growth step sources have implications for the unsteady step dynamics to be discussed below. Since the unsteady behavior depends on the magnitude of the triggering perturbation, these observations indicate that there will always be a source of step density unsteadiness.

B. Kinetics of Step Propagation

1. The Kinetic Coefficient for Incorporation into Steps

The dependence of the step propagation velocity v on the thermodynamic supersaturation $\Delta\mu/k_BT \equiv \sigma$ [$= \ln(C/C_{eq})$] can be postulated as

$$v = \beta_{step}\Omega C\sigma \quad (1)$$

In eq 1, β_{step} is the kinetic coefficient for incorporation into the steps, Ω is the crystal volume per protein molecule, and C is the protein molecular concentration in the solution. Typical Ω values are as follows: for lysozyme, 3×10^{-20} cm^3; for ferritin/apoferritin, 1.56×10^{-18} cm^3; for the satellite tobacco mosaic virus, 4.2×10^{-18} cm^3. This is significantly greater than the value for a typical inorganic system, ammonium dihydrogen phosphate, for which $\Omega = 1.07 \times 10^{-22}$ cm^3. The dimensionless product ΩC accounts for the change in molecular density during crystallization. Typical values vary from 0.06 for a 50 mg/mL lysozyme solution down to 5×10^{-5} for a close to equilibrium 0.023 mg/mL apoferritin solution.

Step velocity is often expressed as a function of the protein concentration in the form

$$v = \beta_{step}\Omega\,(C - C_{eq}) \quad (2)$$

This expression can be derived from basic kinetic principles.[106] However, this derivation requires strong assumptions about the mechanism of incorporation of the molecules into the steps. Molecules are assumed to enter the steps directly from the solution without undergoing adsorption or surface diffusion. As discussed in section II.B.2, for at least two of the proteins studied to date, canavalin and lysozyme, there exists significant evidence that incorporation into steps is preceded by adsorption on the surface followed by surface diffusion. Before sufficient studies are done to confirm that this more complicated growth mechanism is limited to these two cases, the use of the more general expression (eq 1) seems preferable. Of course, given the actual and the equilibrium solution concentrations corresponding to the conditions at which v is determined, one can easily convert from kinetic coefficients determined by eq 1 to kinetic coefficients determined by eq 2. Typically protein crystals are grown at supersaturation levels of $\Delta\mu/k_BT \approx 1-2$ and the ratio $(C - C_{eq})C_{eq}^{-1}/\ln(C/C_{eq})$ is about 5. Thus, the step kinetic coefficient value based on σ should be correspondingly higher than the value based on concentration.

There has been speculation that the growth of tetragonal lysozyme crystals may occur through the incorporation of tetramers or octamers that form in the solution prior to attachment to the crystal.[107−111] The AFM evidence in favor of this hypothesis[109,110] is ambiguous because the experimental resolution required to quantitatively verify this was lacking. Indeed, recent molecular resolution AFM investigations of the crystallization of a number of other proteins show that these grew by incorporation of monomers.[83,112] Furthermore, careful static and dynamic light scattering investigations[24,25,113,114] of the lysozyme solutions from which the crystals grow have not revealed the presence of any species other than the lysozyme monomer.

Measurements of the step kinetic coefficient have been made using interferometric and scanning probe techniques. They involve measurements of step velocity v at 10 different supersaturation levels or protein concentrations. The kinetic coefficient is determined using a fit to an assumed linear dependence of v on σ. Often, the data scatter due to other factors (see argument below) is insufficient to distinguish between eqs 1 and 2.

The values of β taken from the above references are as follows: lysozyme (110) face, 1.4×10^{-4} cm/s; lysozyme (101) face, 2.8×10^{-4} cm/s; ferritin, 2×10^{-4} cm/s; canavalin, $10^{-5}-10^{-4}$ cm/s; satellite tobacco mosaic virus, $(6 \pm 2) \times 10^{-4}$ cm/s; catalase (001) face, 3.2×10^{-5} cm/s; and thaumatin (101) face, 2×10^{-4} cm/s.

Note that eqs 1 and 2 relate the step velocity to the "bulk" protein concentration or supersaturation, i.e., those in the crystallization container far from the crystal. However, the solution that is in contact with the crystal has a different concentration or supersaturation. Protein crystals are typically grown from unstirred solution, which, even in the presence of buoyancy-driven convection, leads to the existence of a zone depleted with respect to the solute at the growth interface. The reason for this depletion is the comparable rates of mass transport to the crystallization interface and through this interface. The characteristic diffusive mass transport rate in the solution $D/\delta = 1\ \mu$m/s $= 1 \times 10^{-4}$ cm/s ($D \approx 10^{-6}$ cm^2/s is a typical protein solute diffusivity, δ ($\sim$0.01 cm) is the transport length scale, commensurate with the crystal dimension). The rate of mass transport through the crystallization interface may be estimated as the ratio of the crystal growth rate R, typically on the order of 10−100 Å/s, to the molecular density change upon crystallization, ΩC, provided above. Values range from 2×10^{-6} to 2×10^{-2} cm/s. The corresponding $R\delta/D\Omega C$ ratios of 0.02 and 200 indicate, respectively, an insignificant $\sim$2% depletion of the interfacial solution with respect to the bulk concentration or purely diffusion-controlled growth regime with a constantly decreasing interfacial concentration. Depleted zones at the protein crystal−solution interface have been experimentally observed using Mach−Zender interferometry and Schlieren techniques to visualize concentration fields around growing lysozyme crystals[115−116] and predicted in detailed numerical simulations of the convective-diffusive transport.[88] This depletion lowers supersaturation at the interface and the steps to move slower than expected based on the bulk driving force. The decrease in step velocity (i) is larger at higher crystal growth rates, (ii) increases with crystals size, and (iii) is location dependent, i.e., facets' centers are exposed to lower supersaturation than the facets' edges, see section II.A.2.

Another factor that may lead to deviations from eqs 1 and 2 is that steps compete for growth material supplied from the bulk solution. The zone of lower solute concentration in the solution around a step

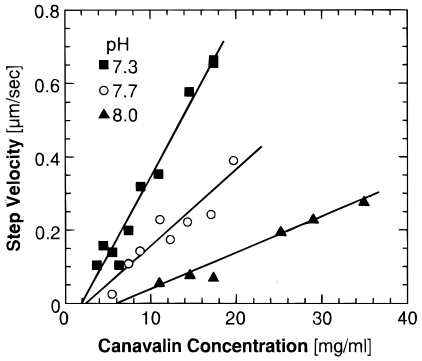

Figure 8. AFM determinations of the dependence of the step velocity on canavalin concentration as a function of pH, as indicated in the plot. (Adapted with permission from ref 118.)

tends to attain the shape of a half cylinder with the step as its axis. If two steps are too close, these cylinders overlap and both steps get less solute than they would if they were far apart. Thus, closely spaced steps move slower that steps further apart. Such dependencies of the step velocities on interstep distance have been recorded for lysozyme[87,92] and canavalin.[118] Scaling arguments suggest[87] that the competition for supply from the bulk should be too weak to cause any discernible effects. Thus, it was assumed that the strong effect of step density on step motion is due to solute adsorption on the interstep terraces followed by surface diffusion toward the steps. The competition for the adsorbed solute molecules between each pair of steps bounding a terrace causes the delay in step motion observed in experiments. For further discussion of this step−step interaction, which is an important component of the nonlinear step dynamics, see section II.B.2.

A third factor is related to the solution behavior of the proteins. The charge on the protein molecules is to a large extent determined by the solution acidity.[119] Thus, it is not surprising that at different pH values the step kinetic coefficient on canavalin crystals was found to be different, see Figure 8 and ref 118.

Besides these intrinsic reasons for deviations from eqs 1 and 2, step velocities may also be affected by impurities. Two mechanisms through which impurities can affect step motion are typically discussed in crystal growth literature. The "stopper" mechanism[120−122] assumes that the impurity molecules are adsorbed on the interface and the steps have to bend to pass between them. The resulting curvature in the step profile increases the chemical potential of the steps, lowers the potential difference that drives step motion, and, thus, slows the steps down. It has been shown that the dependence of step velocity on σ in this case is characterized by a "dead zone" at $\sigma < \sigma^*$ in which no growth occurs. At higher supersaturations $>\sigma^*$, eq 1 or 2 applies, i.e., step velocity is unaffected by the impurities. Evidence for the action of this mechanism has been found for lysozyme, based on averaged (over several hours)[32,33,87,123] and microscopic level[124] kinetics.

The second impurity action mechanism assumes that impurities occupy a fraction of the growth sites

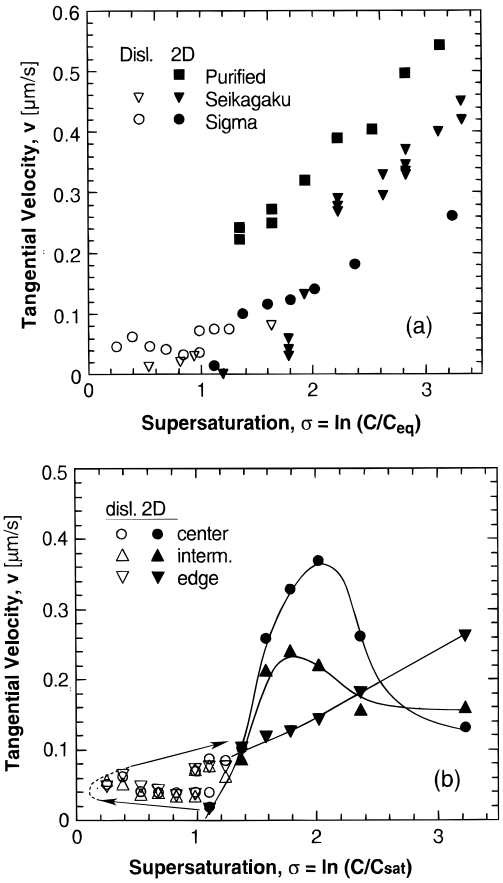

Figure 9. Dependencies of step velocity on supersaturation determined by interferometry: (a) in solutions containing 0.01%, 1%, and 5% (w/v) of other protein impurities (Higher impurity concentration leads to slower step motion). Crystal sizes in all cases <100 μm; (b) at three facet locations, solute and impurities transport conditions altered during the monitoring by the rapid crystal size increase from <100 μm at $\sigma < 1.2$ to above 250 μm at the final data points at $\sigma = 3.25$, arrow indicates sequence of σ changes. (Reprinted with permission from ref 87. Copyright 1996 Elsevier Science.)

at the steps and, thus, decrease the step kinetic coefficient, while the linear relation between the step velocity and the driving force is preserved over the entire range of σ or C.[125,126] Evidence for this type of impurity action has been found during lysozyme crystal growth in the presence of other proteins.[87] The effect of impurities during lysozyme growth are illustrated in Figure 9a, which compares the step velocities measured in three solutions with different impurity levels.

The effects of impurities will also depend on their transport to the growth interface. Figure 9b shows step velocity variations with supersaturation recorded while the crystal dimension in the direction lateral to the observation direction increased significantly. The nutrient solution contains about 5% of other protein impurities that are known to lead to significantly lower growth rates, see Figure 9a. The size increase leads to longer transport lengths and hinders impurity supply to the facet center. As a result, the step velocity at the facet center increases, reaching a maximum at $\sigma = 2.0$, while v only slightly increases at the facet edges that receive better impurity supply. For larger sizes and higher growth

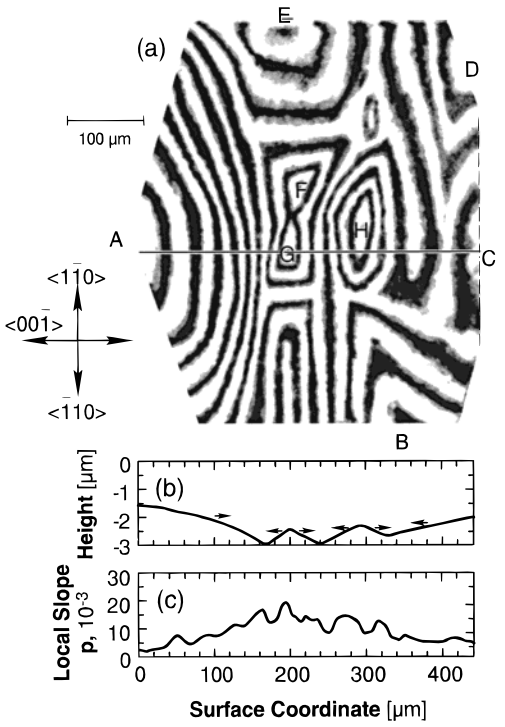

Figure 10. Interferometric visualization of the growth morphology of a (110) face of a lysozyme crystal growing at $\sigma = 2.4$. (a) Interferogram, the interfringe distance in the [110] directions is about twice that along [001], i.e., that the steps propagate half as fast in the [001] directions. In analogy to inorganic systems, this β_{step} anisotropy could either be intrinsic or impurity-induced;[130] dashed line indicates the edge of the viewing field rather than the facet edge). (b) Height profile along the line shown in a with arrows indicating the step motion direction. (c) Magnitude of the vicinal slope p along the line. (Reprinted with permission from ref 92. Copyright 1995 Elsevier Science.)

rates at even higher supersaturations, step velocity is no longer affected by the nonuniform impurity supply,[127] and then the lower supersaturation at the facet center results in lower step velocity.

2. Interstep Interactions

The idea that step−step interactions that exist in some inorganic solution growth systems[128,129] may also be present during protein crystallization is supported by the results of morphology studies. Figure 10 illustrates the morphology of a (110) lysozyme crystal face. Five sources (A−E) along the facet edges and three sources (F−H) in the middle of the facet dominate the layer or step generation. This step source localization is likely associated with higher local densities and/or activities of outcropping defects, see section II.A.2, or to the higher σ's at the edges.

Figure 10b shows the height profile, calculated as in ref 34, along the line indicated in Figure 10a. The local vicinal slope p in Figure 10c is about 4 times lower at the facet edges than at the facet center. Measurements of the step velocity at various locations showed a 4-fold decrease of v from edge to center, independent of step propagation direction. The product of p and v, the growth rate R, is thus uniform over the facet.

Although the convex shape in Figure 10 agrees qualitatively with the expected stabilization mechanism through slope variation,[131,132] the large values of p_{center}/p_{edge} (~4) in Figure 3 pose an interesting problem. According to the simple model for slope readjustment to accommodate lower supersaturation at the facet center, such low slope ratios would indicate differences in interfacial supersaturation between the center and corner of several hundred percent. However, model calculations,[88] based on realistic kinetics and transport parameters for lysozyme, predict σ nonuniformities over the facet of less than 20%. A qualitative explanation is that as the step density (slope) increases in response to the lower supersaturation, the steps slow due to increasing overlap of their nutrient field. This further decreases the distance between them and, thus, increases the slope.

Further independent evidence for the overlap of step diffusion fields was deduced from a dissolution experiment (step motion in dissolution is considered symmetrical to that in growth[133,134]) with a flattened crystal facet. Etching at low supersaturation left the central regions flat. This means that the steps that were present on the facet prior to etching remain essentially equidistant, indicating the absence of interfacial σ-nonuniformities. At the same time, etching steps formed at the edges moved inward. The resulting edge profile had a gradual decrease in slope from edge to center from $p_{high} \approx 40 \times 10^{-3}$ to $p_{low} = 6 \times 10^{-3}$. Since the step generating capacity of the edges is constant, the probable reason for the spatially decreasing slope is an overlap of the step diffusion fields, see model in ref 133. Further evidence in support of interstep interaction is discussed in section IV.A.

Assuming incorporation into steps from the surface following serial volume and surface diffusion,[136,137] the requirement that the slope ratios in Figure 10 be reproduced leads to some very reasonable values of the kinetic parameters. A reasonable presentation of the rather cumbersome relation in ref 136 would be

$$v = \frac{b_{step}\sigma}{1 + kp} \tag{3}$$

where $b_{step} = \lambda_s^2 D\Omega C/\Lambda_s h$ is an effective step kinetic coefficient and $kp = (\lambda_s^2/\Lambda_s h)(1 + \delta/\Lambda)p$ is a dimensionless number characterizing the relative importance of the bulk and surface diffusion for step propagation. Λ is the resistance for adsorption to the surface, Λ_s is the resistance for incorporation into the step from the adsorbed state, λ_s is the characteristic surface diffusion length, and h is the step height. In the terms of eq 3, the requirement for step field overlap is $kp \approx 1$. If bulk transport is fast or if step motion can be correlated with interfacial protein concentration, $\delta = 0$.

The only other protein crystallization system for which interactions between steps have been systematically studied is canavalin.[118] The results of in-situ atomic force microscopy investigations and a simple diffusion analysis suggest that surface diffusion,

Figure 11. AFM image of a growth spiral on a canavalin crystal. Two dislocations with closely located outcrops produce two steps. A third dislocation outcrops to the upper right of these two. The steps generated by the first two dislocations propagate toward the facet periphery. Initially, the two steps are close. As they move on, the distance between them increases and becomes equal to half the spiral step. (Adapted with permission from ref 118.)

rather than bulk diffusion, is the controlling mechanism of solute transport to the steps. The strongest evidence in favor of this claim is the homogenization of an initially nonuniform double-step train, Figure 11. Here the dislocation step source on top of a hillock has a value of 2 unit step heights. It produces two, initially coupled steps. The difference between the two steps is that the upper step has a narrow terrace at its lower edge while the lower step has the same narrow terrace at its upper edge. Gradually, as the steps move away from their source, the terrace widths homogenize. Bulk diffusion alone is unlikely to account for this homogenization. The bulk supply fields to these steps are identical, and with or without bulk diffusion field overlap, the steps should remain coupled. Solution flow in the direction opposite to step motion could result in homogenization.[138,139] However, homogenization is observed in all directions. As with the lysozyme results above, these observations could be explained not only qualitatively but also quantitatively, simply by assuming asymmetry of the kinetic coefficient of incorporation into a step from the left and from the right terrace (the Schwoebel effect[140,141]). More importantly, such asymmetry is only possible if incorporation into the steps occurs via a multistage process involving adsorption on the interface and surface diffusion toward the steps.

The interaction between steps through overlapping of their surface diffusion fields discussed in the above subsection is an important factor in the nonlinear dynamics of steps that causes the unsteady behavior discussed below.

III. Defects, Strain, and Molecular Disorder in Protein Crystals

All defects known for inorganic crystals, such as point defects (vacancies, interstitials, or incorporated impurity species) as well as dislocations, grain and twin boundaries, occlusions of mother liquor and crystallites, occur in protein crystals. Some of the mechanisms that lead to the creation of such defects were discussed in section II.A.1. X-ray projection topography[142] has been used to visualize their locations and distributions in the crystals.[143−147] All studies reflect the relatively high strain levels of the protein crystals as compared to inorganic crystals, which cannot always be correlated to the presence of any of the linear, planar, or 3D defects. Such high strain levels can be attributed to nonuniform impurity incorporation or to molecular disorder in the crystals. Nonuniform distribution of impurities is associated with unsteadiness in growth kinetics (see section IV.B) that may occur at various stages of the growth due to different reasons. For instance, higher impurity amounts in the central regions of lysozyme crystals and associated higher precipitant concentrations have been inferred from combined chemical−biochemical and X-ray topography studies.[148] These findings were recently supported by the results of a fluorescence investigation of impurity distribution.[149] As discussed in section IV.B, unsteady kinetics and step bunching may also cause nonuniform defect and impurity incorporation in the crystals.

To characterize crystal quality, X-ray rocking curve widths have been determined for many of the crystals discussed above. It was noted that these widths are about an order of magnitude higher than expected for perfect protein crystals. This was attributed either to higher elastic strain in the crystals or to a block structure of the studied specimens. There has been considerable discussion about the correlation between the rocking curve widths and the diffraction resolution limits. Clearly, higher rocking curve width means broader diffraction spots, lower accuracy of the determination of their coordinates, lower ratio of the maximum intensity in a spot to the surrounding noise, and, hence, lower resolution.[150,151] This seems to be especially true for crystals that exhibit broadening due to strain. However, if the wide rocking curves are due to block structure, the beam in a X-ray diffraction arrangement can be focused on only one of these blocks and high-resolution structure determinations can still be achieved.[152]

The size of the protein molecules is about an order of magnitude larger than the range of interactions between them.[106] If recalculated per unit contact area, the strength of these interactions is also rather low. This is considered to be one of the reasons for the relatively slow protein crystal growth kinetics and may also underlie the presence of an imperfection unique for this type of crystals: rotational disorder of the protein macromolecules. This disorder has been studied by electron microscopy of freeze-etched and metal-decorated crystals.[153] This technique is based on coating under vacuum of frozen-hydrated protein crystals with a few monolayers of a low melting metal, such as Au or Ag. The distribu-

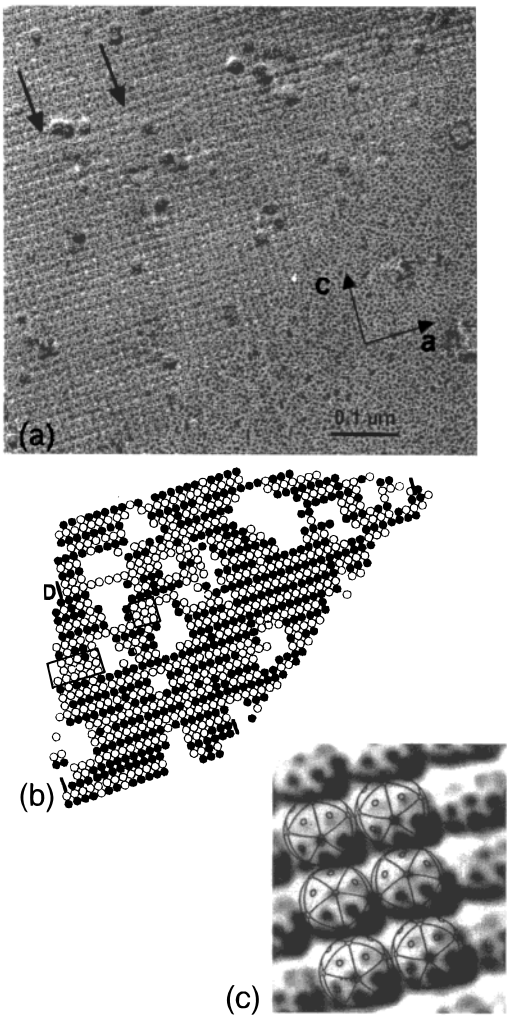

Figure 12. Silver-decorated (010) face of a lumazine synthase crystal. (a) Distribution of silver spots along the surface, from which the orientation of the individual molecules can be deduced. As shown in c, in this crystal molecules take one of two orientations: with the 5-fold axis upward, represented by black circles in b, or with the 5-fold axis tilted forward, open circles in b. (b) Schematic illustrating the distribution of the two molecular orientations on the surface. Perfect crystals exhibit alternating "white" and "black" molecular rows, deviations from this pattern indicate molecular disorder. Arrows in a and rectangles in b highlight locations of accumulated misoriented molecules. (Adapted with permission from refs 155, 160, and 162.)

tion of the metal clusters on the surface of the protein is related to the topochemistry of the molecule's surface.[154] This technique was used to study two- and three- dimensional crystals that allow an averaged decoration pattern to be identified[155−158] as well as noncrystalline specimens.[159,160] On the decoration pattern, various features of the packing of the top crystallographic plane can be visualized, including the rotational orientation of the individual molecules.[161] When this technique was applied to, among many others, hexagonal crystals of lumazine synthase, it was found that the surface molecules on an undisturbed surface adopted two possible orientations in an alternating manner according to the crystal packing, Figure 12. Orientational disorder was observed at and around a dislocation, where patches of molecules showed "wrong" orientations.[162] Similarly, the molecules on the surface of ferritin crystals seemed to possess no orientational order.[162]

These results on the molecular orientational disorder in protein crystals, although still limited to only a few materials, indicate that even if it were possible to grow the crystals from a perfectly pure solution, defects and related strain can still be introduced and compromise the crystal's utility.

IV. Unsteady Growth Kinetics and Step Bunching

A. Phenomenology and Dependence on Transport Parameters

Interferometric monitoring of the local growth rate R, vicinal slope p, and tangential velocity v during the growth of lysozyme revealed that the growth variables are not steady and fluctuate by as much as ∼80% of their average values, Figures 13 and 14.[163] The variations in p, which is proportional to the step density, indicate that the fluctuations are due to the passage of step bunches, i.e., the steps on the interface are not equidistant but rather grouped into a pattern of lower and higher step density. An example of such a wave of high step density moving on a crystal of another protein, ferritin, is shown in Figure 15.

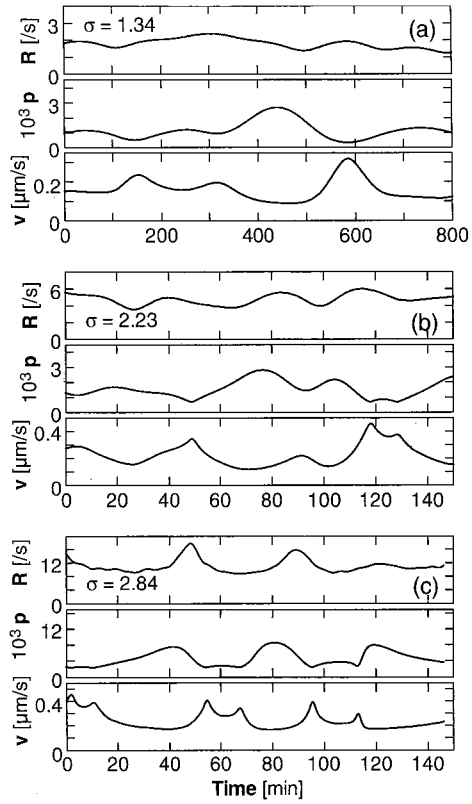

Figure 13. Time traces of normal growth rate R, local slope p, and tangential (step) velocity v recorded at center of the {110} facet of the same crystal at three supersaturations, indicated in the plots. Crystal size ∼250 μm. The local determinations of R represent integrals of the interferometric intensity over interfacial areas of ∼0.5 × 0.5 μm^2, while the p values are averaged over distances of ∼3 μm; see ref 34. The solution temperature in the cell was uniform and stable within 0.01 °C. (Reprinted with permission from ref 163. Copyright 1996.)

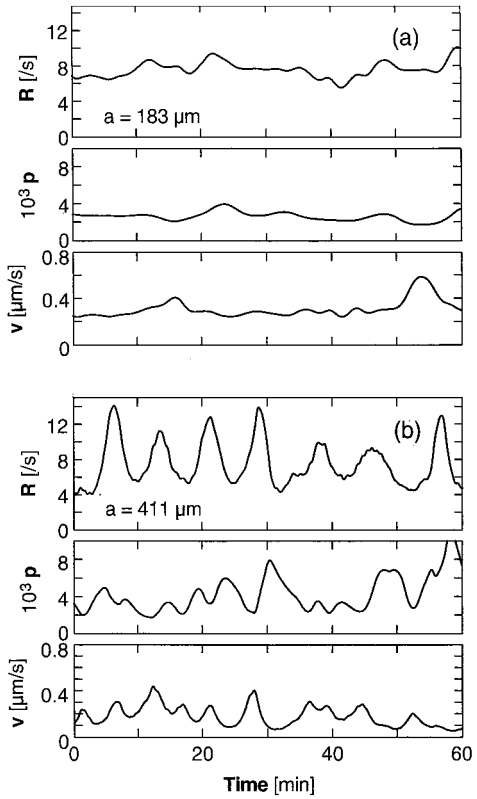

Figure 14. Increase of fluctuation amplitude at facet center location with crystal size a, indicated in the plots; $\sigma = 2.84$. (Reprinted with permission from ref 163. Copyright 1996 American Physical Society.)

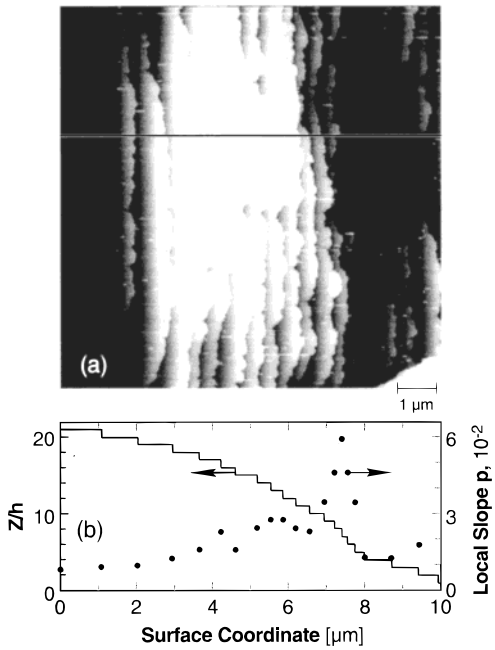

Figure 15. AFM imaging of a step bunch propagating on the surface of a growing apoferritin crystal. (a) AFM image, individual growth steps move from left to right. (b) Interface profile showing the nonuniform distribution individual growth steps 106 high and local slope along line in a. (Adapted with permission from ref 83.)

The excursions of p and v tend to be in opposite directions: high and low step densities are associated, respectively, with low and high tangential velocity. This indicates strong overlap of the steps' nutrient supply fields (see section II.B.2). Tests using solutions of three distinct purity levels, (i) as supplied by Sigma and (ii) by Seikagaku and (iii) Seikagaku lysozyme purified to 99.9% with respect to higher molecular weight proteins,[56] showed no dependence of the fluctuations on solution purity.

The characteristic fluctuation time Δt (average time between major excursions) is on the order of 10 min. For comparison, the characteristic step generation time $\tau_{step} = h/\bar{R}$ with the step height h of at most a few hundred Å and the average growth rate $\bar{R}$ of some 10 Å/s is on the order of 10 s. Hence, in contrast to the findings with barium nitrate and potash alum,[164,165] the fluctuation time scales are at least several 10 times longer than τ_{step}. However, in another investigation, barium nitrate showed fluctuations in R with 1 min $< \Delta t <$ 10 min,[166] which were interpreted in terms of moving multidislocation step sources of varying activity. With lysozyme, Δt's obtained with 2D nucleation- or dislocation-step sources were comparable. Therefore, we conclude that these fluctuations are not merely a reflection of the dynamics of multidislocation step sources, though they may affect them.

Figure 13 shows fluctuation traces recorded at the same location of a crystal at increasing supersaturations. Note that the fluctuation amplitude of both p and v is independent of σ. At low σ, $v(t)$ and $p(t)$ are largely in counterphase. With increasing σ, the phase difference between fluctuations in v and p becomes random. Consequently the R excursions increase. The characteristic time of the fluctuations Δt (average time between major excursions) decreases with supersaturation. At $\sigma = 2.84$ (Figure 13c), Δt drops to <10 min. In other experiments at comparable or higher supersaturations, Δt's as short as 5 min have been observed. Figure 14 shows a comparison between the fluctuations observed at the facet center for two different crystal sizes a. The variations in R, p, and v and the fluctuation frequency significantly increase with a.

As observed in Figure 13, at higher supersaturations the fluctuation amplitude of R increases more than those of p and v. This can be understood in terms of transport considerations. Expanding $v(t)$ in $R(t) = p(t)v(t)$, the growth rate R at any point on the interface can be written as

$$R(t) = p(t)b[p(t)]\sigma_s(t) \qquad (4)$$

where $b(p)$ is a kinetic coefficient for incorporation of growth units into steps and σ_s is the supersaturation at the interface. In this system, $b(p)$ decreases with increasing p due to the overlap of the steps' (surface) diffusion fields, see section II.B.2. At low average growth rates, there is sufficient time after the passage of a step bunch for the local σ_s to recover. Hence, the local σ_s is not affected significantly by variations in step density. As a consequence, the opposing deviations in p and $b(p)$ largely compensate. This yields a nearly steady R. At higher average R, however, the local σ_s is strongly modulated by the passing step bunches. This results in v fluctuations that are out-of-phase with those in p, leading to pronounced nonsteady R.

More formally, the relation between the changes in the surface supersaturation and normal growth rate can be understood if one considers the time derivative of eq 4

$$\frac{\partial R}{\partial t} = \left[\left(\frac{1}{p} + \frac{1}{b}\frac{\partial p}{\partial t}\right)\frac{\partial p}{\partial t} + \frac{1}{\sigma_s}\frac{\partial \sigma_s}{\partial t}\right] R \tag{5}$$

or

$$\frac{1}{R}\frac{\partial R}{\partial t} = \left(1 + \frac{p}{b}\frac{\partial b}{\partial p}\right)\frac{1}{p}\frac{\partial p}{\partial t} + \frac{1}{\sigma_s}\frac{\partial \sigma_s}{\partial t} \tag{6}$$

Here

$$b(p) = b_0(1 + kp)^{-1} \tag{7}$$

where k is a (surface diffusion) step interaction parameter see eq 3. We consider systems for which, see section II.B.2,

$$kp \gg 1 \tag{8}$$

It then follows that

$$\frac{p}{b}\frac{\partial b}{\partial p} \approx -1 \tag{9}$$

Equation 9 reflects the observed compensation of the opposing p and v fluctuations due to the strong interstep interaction expressed by eq 8. Thus, the first term on the right-hand side of eq 6 is vanishingly small and

$$\frac{\partial R}{\partial t} \approx \frac{R}{\sigma}\frac{\partial \sigma_s}{\partial t} \tag{10}$$

As a consequence, in the absence of σ_s modulations, R should be steady even though p and v fluctuate.

Furthermore, we can show that even under conditions that do not induce R fluctuations, step bunches that lead to variations in p may still form. From eq 5, with $\partial R/\partial t = 0$

$$\frac{1}{p}\frac{\partial p}{\partial t} \approx \left(1 + \frac{p}{b}\frac{\partial b}{\partial p}\right)^{-1}\frac{1}{\sigma_s}\frac{\partial \sigma_s}{\partial t} \tag{11}$$

In contrast to eq 10, the action of $(\partial\sigma_s/\partial t)$ upon $(\partial p/\partial t)$ is amplified by the large value of $[1 + (p/b)(\partial b/\partial p)]^{-1}$. Thus, even small perturbations in σ_s that do not result in significant R fluctuations may lead to significant fluctuation in local slope/step density. In addition, eq 11 helps to explain the significance of step field overlap for step bunch formation and ultimately for the kinetics fluctuations. If the condition of eq 8 is not satisfied, $0 \geq (p/b)(\partial b/\partial p) \gg -1$ and small σ_s perturbations may only lead to insignificant p variations. This is similar to the interstep interaction effects on microscopic morphology formation on a much larger length scale. In the latter case, supersaturation nonuniformities of ≤10% between facet center and edge induce up to 5-fold increases in average slope, see section II.B.2 and refs 92 and 167.

B. Correlation between Unsteady Kinetics and Crystal Imperfections

Although kinetics unsteadiness, step dynamics, and step bunching are an intriguing area of research, these results would only be relevant to the goal of other protein researchers if the unsteady kinetics causes significant deterioration of crystal quality. In search of a spatiotemporal correlation between growth rate fluctuations, step bunching, and striations in the crystals, similar to that found in semiconductor crystallization,[168] a few crystals were nucleated on a horizontal glass plate in the growth cell. Since lower solution purity enhances the visibility of striations,[87] protein material with ~1% of covalently bound lysozyme dimer was used.[56] After 1.5 h of interferometric monitoring of a suitably positioned (110) face, the cell was opened and the glass plate was turned vertically since visualizations of the striae (microscopically thin layers of defects) require viewing in a direction parallel to the plane in which they lie. To avoid solution evaporation and optical distortions from curved liquid−air surfaces, the cell was closed and refilled with solution.

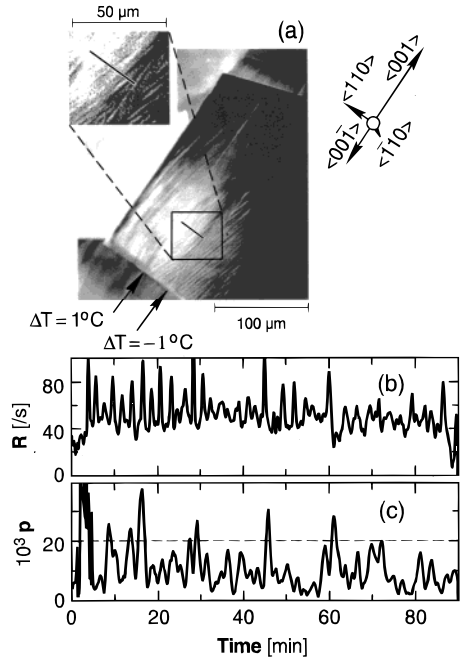

Figure 16. (a) Polarized light reflection image of the crystal viewed in a direction parallel to the monitored face, with the focal plane positioned in about the middle of the crystal. (Insert) 2:1 enlargement of the squared area with enhanced contrast to better visualize the striations. Lines indicate location of interferometric monitoring. Arrows point to striations caused by $|\Delta T| = 1$ °C before and after monitoring. Orientation of crystallographic axes is shown on the right. Time traces of (b) growth rate R and (c) vicinal slope p recorded at the location corresponding to lines in a at $\sigma = 1.9$ ($T = 20$ °C). (Reprinted with permission from ref 169. Copyright 1998 American Physical Society.)

The interfacial interferograms of the (110) face indicated that the growth steps are generated at the facet center and mostly spread toward the ⟨001⟩ and ⟨00$\bar{1}$⟩ directions.[169] Figure 16a presents a polarized light micrograph of the grown crystal viewed parallel to the interface. The two straight striations were intentionally induced by a 1 °C temperature change[170] to mark the beginning and end of the interferometric data collection. In this low-resolution view, these markers appear parallel to the (110) plane. Between the markers, in the lower, left region, one can discern a system of closely spaced, inclined striations. The

inclination with respect to the (110) plane is between 10° and 15°. This corresponds to striae originating at macrosteps which should be inclined with respect to the singular plane by an angle α, related to the local normal growth rate R and step bunch velocity v_{bunch} by

$$\tan \alpha = R/v_{bunch} \quad (12)$$

Substituting the interferometrically determined values from Figure 16b,c (for details, see ref 34) yields $\alpha \approx 14°$, well within the range extracted from Figure 16a.

For further evaluation, an enlarged image was used with the black line in both images indicating the 32 μm displacement of the interferometric observation location during the measurement period. About six striations cross this line of growth between the markers in Figure 3a with an average spacing Δx of 5−6 μm. The number of striations equals the number of step bunches with slope $>2 \times 10^{-2}$ in the respective local slope time trace in Figure 16c. Furthermore, the heavier striations at the beginning of the monitoring interval correspond to steeper step bunches.

A more quantitative correlation between the optical image of the striations and the vicinal slope trace $p(t)$ is hampered by the nonlinearities involved in the striation imaging process in Figure 3a. Furthermore, the step orientation, density, and number of the step bunches may vary in the direction perpendicular to the step motion direction (for numerous examples of such step patterns, see ref 168). This would lead to variations in the optical thickness of the trailing striations, whose projection on the $(\bar{1}10)$ plane is visualized in Figure 16a.

Yet, based on the above material, the formation of compositional inhomogeneities in lysozyme crystals grown under steady solution conditions can be clearly correlated with the intrinsic instabilities of layer growth dynamics. It may not be obvious how inhomogeneities on the micrometer scale may affect the diffraction resolution obtainable from a crystal in the sub-3 Å range. For this reason, it is important to note that the maximum diffraction resolution is determined by the signal-to-noise ratio of high-index reflections. Since high-index crystal planes have low molecular density, much wider areas of rotationally and translationally aligned molecules are needed to enhance the intensity of the reflections from these planes and increase their signal-to-noise ratios. Hence, crystal imperfections on the scale of micrometers (e.g., striations discussed here) and even tens and hundreds of micrometers (block structures, twins, etc.) affect the diffraction resolution that can be obtained from a given crystal.

Another problem associated with step bunching is the possibility of their evolution into overhangs, Figure 17a.[171] These arise because of the higher supersaturation of the solution at locations further from the interface, into which the step bunches protrude. These overhangs may close, forming a line of solution occlusions parallel to the step. Occlusions of nutrient solution may also result from the loss of lateral stability of the step bunch itself, Figure 17b.[172,173] In this case, the lines of occlusions are often perpendicular to the steps.

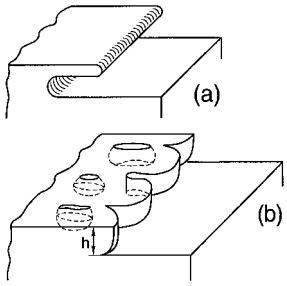

Figure 17. Evolution of step bunches: (a) Overhang that may collapse and form a line of inclusions parallel to the steps; (b) Development of a cellular structure after the lateral loss of stability. (Adapted from ref 171.)

The results presented in this subsection indicate that the kinetics fluctuations and the underlying step bunching have detrimental effects on the quality and likely on the utility of the growing crystals. Hence, the mechanisms leading to such instabilities should be studied further so that a means to minimize and possibly eliminate them could be identified.

C. Macroscopic Models of Kinetics Unsteadiness and Feasibility Tests

1. General Considerations

In section IV.A, it was shown that the R, v, and p fluctuation amplitudes depend on the supersaturation (average growth rate) and crystal size. These are the variables that also strongly influence the local transport conditions at the interface.[90,91,174] The above observations have been interpreted in terms of the nonlinear dynamics of coupled transport and surface kinetics (see discussions in refs 175−181). Since no impurity effects on the fluctuations were found, it was concluded that the observed fluctuations are intrinsic to the system. Such intrinsic fluctuations occur in many systems (physiological, biological, chemical, and mechanical) that operate far from equilibrium.[182]

Macroscopic theoretical treatments of rate fluctuations in phase transformations have assumed that bulk and interfacial processes are coupled. Furthermore, it is assumed that the bulk transport rate is a linear function of the bulk solute concentration and interfacial processes may be nonlinear functions of the interfacial concentrations of the participating species. Nonlinearities in interfacial kinetics can be caused by chemical reactions that precede or compete with incorporation into the crystal,[175,176] impurity effects, or a delay in the interface response to a perturbation in the local concentration of a component.[177] The coupling of linear and nonlinear processes results in unsteady rates with time constants largely exceeding those of the individual steps.[183] The general trend that emerges from the above models[177] is that for growth under pure kinetics or transport control, where the interfacial concentration C_s approaches, respectively, the bulk concentration C_∞ and equilibrium concentration (solubility) C_{eq}, the system is steady and all perturbations are damped. For mixed control, however, the system is unsteady and

fluctuations about a mean rate occur. Maximum response occurs if surface kinetics and transport have a comparable influence on the overall growth rate.

The control parameter for the interfacial instability can be expressed as a kinetic Peclet number, which is the ratio of the rate constants for nonlinear incorporation kinetics and bulk transport in the form

$$Pe_k = \beta_f \frac{\delta}{D} \tag{13}$$

where β_f is the face kinetic coefficient, D is the solute diffusivity, and δ is a characteristic diffusion length (commensurate with the crystal size). Values of $Pe_k \ll 0.1$ or $\gg 1$ indicate, respectively, purely kinetic or transport-controlled growth in which perturbations are damped and growth is steady. Intermediate values characterize mixed growth control for which both kinetics fluctuations and step bunching occur. This criterion for the conditions that lead to damping of growth perturbations can also be interpreted in terms of the surface concentration C_s. This follows from the fact that within certain general assumptions[184]

$$C_s \approx C_\infty - (C_\infty - C_{eq}) \frac{Pe_k}{1 + Pe_k} \tag{14}$$

Thus, if $Pe_k \to 0$, $C_s \to C_\infty$, and if $Pe_k \to \infty$, $C_s \to C_{eq}$. For more details on these findings and additional references, see ref 163.

2. Numerical Model

For a feasibility test of this unsteady kinetics mechanism, the transport fields from the bulk of a solution to individual growth steps moving on a faceted crystal were numerically simulated. Nonlinearity in the interface step kinetics is introduced through a parameter for the overlap of the steps' surface diffusion fields.

The geometry of the transport model is based on the setup used in experimental investigations.[34] As depicted in Figure 18a, the crystallization cell is approximated by a 2D closed domain of 1 mm height and 6 mm width. A crystal of fixed size, 0.6 mm wide and 0.3 mm high, rests on the middle of the cell bottom. The initial lysozyme mass concentration in the solution is $C = 50$ mg/mL. At 12 °C, this gives rise to an initially uniform value of the supersaturation $\sigma_0 = 2.78$.

As indicated in Figure 18c, the solution−crystal interface initially consists of equidistant microscopic growth steps of height $h = 108$ Å ≈ 0.01 μm with singular terraces between them. With an initial vicinal slope of the interface $p_0 = 5 \times 10^{-3}$,[87] about 140 equidistant steps cover the half-facet at the beginning of a simulation. Only diffusive transport of solute to the growth steps was considered. To resolve the concentration field about individual growth steps, a mesoscale subdomain above the interface was introduced, see Figure 18b. For the transport calculations, the actual vicinality of the interface is ignored and the steps are assumed to move within a singular horizontal interface, which is represented by the heavy horizontal line in Figure 18b. The interfacial concentration boundary condition for the domain is tied to the protein consumption at the moving steps.

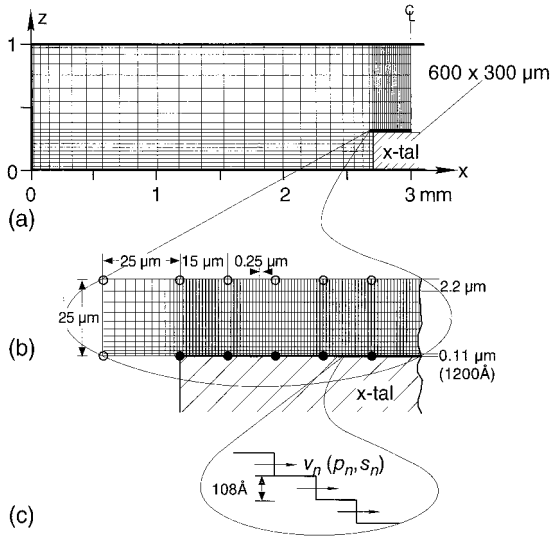

Figure 18. Geometry and grids used in the simulations: (a) bulk (global) mass transport, 45 × 21 grid; (b) interfacial (mesoscale) subdomain, 1221 × 21 grid; (c) steps moving in interface (heavy black line in Figure 1b). (Reprinted with permission from ref 185. Copyright 1997 American Physical Society.)

On the basis of the evidence reviewed in sections II.B.1 and II.B.2, the velocity of the steps was assumed to follow the relation

$$v(n) = \frac{b_{step}\sigma^s(n)}{1 + kp(n)} \tag{15}$$

where b_{step} is the step kinetics coefficient and $\sigma^s(n)$ is the interfacial supersaturation at the nth step. The group $kp(n)$, with $p(n)$ being the slope about the nth step, accounts for the mutual deceleration of adjacent steps through overlap of their surface diffusion fields. The stronger the competition for nutrient among neighboring steps, i.e., the larger $kp(n)$, the lower is $v(n)$.

The specific form of eq 15 for the nonlinearity in interfacial kinetics is based on the experimental observations with lysozyme and NaCl as the precipitant. Note that a different solution composition and, thus, possibly different interfacial kinetics could result in a different form of eq 15. Hence, different fluctuation amplitudes and time scales can be expected for other systems.

Growth on a facet ceases when all initially imposed steps have reached the center and the facet has become singular. That is, growth can only be sustained through the replenishment of growth steps. Hence, in accordance with recent findings for lysozyme, section II.A.2, it was assumed that at the σ's used in our simulations, growth steps are generated by 2D nucleation at the edge of the crystal, where the supersaturation is the highest. For details of the stochastic nucleation formulation, the mesh sizes in the bulk and ms domain, the numerical approach, and the matching of the simulation data to the

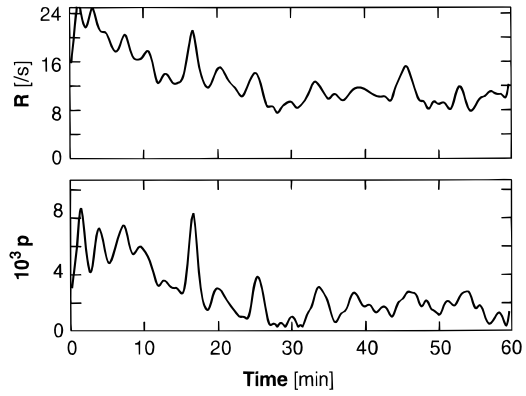

Figure 19. Growth rate $R(t)$ and slope $p(t)$ obtained in simulations with stochastic nucleation mode, $k = 500$, and $D = D_{lysozyme}$ at the middle of the half-facet after data processing to reduce spatial resolution to those of our experiments. (Reprinted with permission from ref 185. Copyright 1997 American Physical Society.)

limited spatial resolution of the experiments, see ref 185.

3. Simulation Results

Results for $R(t)$ and $p(t)$ obtained in the middle of the half-facet (150 μm from crystal corner) using the diffusivity of lysozyme and an experimentally determined step interaction parameter $k = 500$ are shown in Figure 19. Note that in contrast to the experimental results (Figures 13 and 14), both the average growth rate and slope obtained from the simulation systematically decrease. This is due to the larger ratio of crystal "surface area" to solution "volume" in the 2D simulation model. As a consequence, the bulk supersaturation and, thus, the theoretical value of R decreases more rapidly than the experimental one.

From the $p(t)$ trace in Figure 19, one sees that the growth rate fluctuations are due to the passing of step bunches. The characteristic time between the passage of major step bunches is several minutes. This is again about 2 orders of magnitude longer than the average step generation (nucleation) time of ~5 s. To facilitate their quantitative comparison, we have decomposed the simulated and experimental $R(t)$, respectively, into their Fourier components, see Figure 20. To correct for the model-induced decrease in average growth rate, the four lowest frequency components were disregarded, see the dashed lines in Figure 20a. The inset in Figure 20a shows $R(t)$ after deduction of these lowest components, together with a trace resulting from the superposition of these components alone. In comparing parts a and b in Figure 20, one sees that the simulation reproduces both the amplitude and characteristic time of the R fluctuations observed in the experiments rather well.

To test the supposition that the fluctuation amplitude depends on both the nonlinearity of the interfacial kinetics and the relative importance of bulk-transport and interface kinetics, the model input parameters were varied. It was found that shifts toward kinetics control drastically reduced the amplitude of the fluctuations. Similar reductions in the

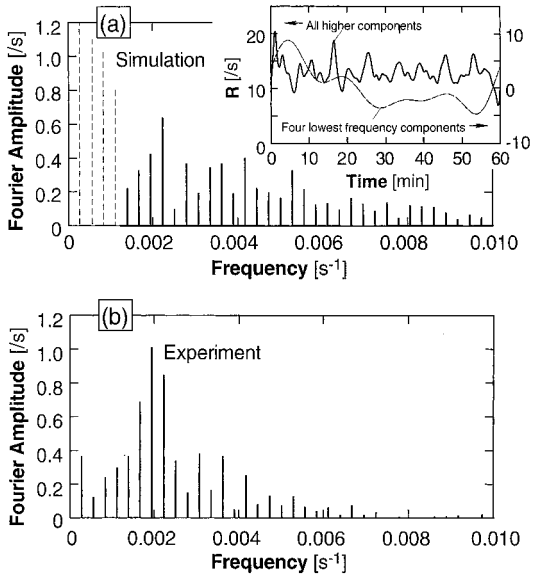

Figure 20. Fourier decomposition of $R(t)$. (a) Simulation results: (inset) subtraction of the four lowest frequency components of $R(t)$, for details see text. (b) Experimental results. (Reprinted with permission from ref 185. Copyright 1997 American Physical Society.)

fluctuation amplitude were encountered on setting the step surface interaction parameter in eq 13 to zero. Thus, the simulations unambiguously confirm that in analogy to the unsteady behavior of other systems involving coupled bulk-transport and nonlinear kinetics (see section IV.C.1), both the nonlinearity in growth step kinetics and mixed transport/kinetics control of the crystallization process are necessary conditions for the growth rate fluctuations.

Further simulations shed light on the microscopic evolution of the fluctuations and step bunches.[185] It was established that the fluctuations are associated with morphological instability of the vicinal face, in which a step bunch (macrostep) triggers a cascade of new step bunches through the microscopic interfacial supersaturation distribution. This behavior is well described in terms of the kinematic wave theory[186] that relates step flow during the growth of crystals to equations used to describe traffic flow.[187−189]

V. Microscopic Mechanisms of Instability and Step Bunching

A. Linear Stability Predictions

Numerous microscopic models for unsteady growth involve the formation, stability, and decay of step bunches (macrosteps). Stimulated by detailed observations of various step patterns,[190,191] dynamic step bunching has been associated with surface diffusion[191−194] and different kinetic coefficients for incorporation into a step from the upper and the lower terrace (the Schwoebel effect.[140,141]

Of particular importance for this investigation is an analysis of the stability of an equidistant step train under convective−diffusive solute transport to infinitesimal perturbations.[138,195−198] It was found that convective flow affects the development of

macrosteps if

$$u_\infty \gg v_{ph} \tag{16}$$

and

$$u_\infty \lambda_0 / D > 1 \tag{17}$$

where u_∞ is the bulk solution flow velocity parallel to the interface and v_{ph} is the phase velocity of the step density wave with wavelength λ_0. For order of magnitude estimates, v_{ph} is assumed to be comparable to the average step velocity $\bar{v}$. It is important to note that the flow direction plays a crucial role for the stability of the step train. Solution flow in the direction of step motion causes step bunching in response to perturbations with λ longer than

$$\lambda_c^f = 2.51 \bar{p}^{-3/2} \sqrt{\frac{\delta D}{u_\infty}} \tag{18}$$

where $\bar{p}$ is the average slope of the vicinal face considered. Solution flow opposite to step motion suppresses bunching. This behavior was observed in forced solution flow experiments with ammonium dihydrogen phosphate crystals.[195]

Buoyancy-driven flow, which, due to solutal density gradients, is always present in terrestrial solution-growth systems, can also affect the stability of step trains. In most inorganic systems, however, the inequality in eq 16 does not hold in unstirred solutions. Typical values of u_∞ are on the order of a hundred μm/s,[199] i.e., comparable to characteristic v's.[128,129] In contrast, protein systems, due to their slow interface kinetics, could provide an opportunity to observe such interactions between natural convection and step motion. For instance, for lysozyme, $\bar{v}$ is typically 0.05−0.5 μm/s[32,33,80] while u_∞'s are about 10 μm/s.[88,115] With this u_∞, $D = 0.73 \times 10^{-6}$ cm^2/s,[24] and observed step bunching wavelength $\lambda_0 = \bar{v}\Delta t$ of about 50 μm, we get $u_\infty \lambda_0 / D \approx 7$. According to eq 17, step trains should be affected by buoyancy-driven flows. This should reduce the macrostep height along step trains moving from the center to the periphery of a horizontal facet since, in this case, the natural convection flow is opposite to the step motion.[88,200] On the other hand, as step bunches move toward the center of a horizontal facet, their height can be expected to increase. At the same time, evaluation of eq 18 for lysozyme, with $\bar{p} = 5 \times 10^{-3}$ [87] and $\delta = 200$ μm,[88] yields a flow-induced critical wavelength $\lambda_c^f \approx 30$ cm. Since this is orders of magnitude larger than the typical crystal sizes of O (100 μm), it is unlikely that the fluctuations observed with lysozyme are caused by flow-step train interactions.

These model analyses were further improved to include stagnant solutions with purely diffusive transport as well as mutual retardation of steps due to their supply field overlap.[198] The resulting equations cannot be solved in closed form without oversimplifications. Thus, the only way to compare a group of experimental results to theory is by solving the governing equations numerically. When this was done for lysozyme crystal growth, the instability wavelengths and frequencies observed in the experiments and simulations, reviewed above, were quite different from those predicted by linear stability analysis of step motion in flowing and stagnant solutions.[201] Hence, the causes for the unsteadiness observed in ref 163 should be sought elsewhere.

B. Numerical Simulation of Suspected Incorporation Pathway

In view of the failure of linear stability analyses to account for the experimentally observed unsteadiness, the evolution of step bunches triggered by perturbations of different amplitude was simulated numerically. Such an evolution may involve a nonlinearly amplified response to small-scale perturbations. Since sequences of kinetic processes are particularly prone to respond nonlinearly, all currently known stages of the growth mechanism were included in the model. For this reason, the model of coupled bulk-transport and interfacial kinetics (see section IV.C) was extended to explicitly include solute adsorption on interstep terraces, surface diffusion, and desorption or incorporation into steps. Direct incorporation from the solution into steps was ignored, since it was shown that it is of negligible significance to the interstep interactions (see section II.B.2 above and ref 92).

The geometry of the diffusive bulk transport is the same as that in section IV.C. The volume−surface exchange process is governed by the interfacial boundary condition

$$D \left.\frac{\partial C}{\partial z}\right|_{intf} = \left(\frac{D}{\Lambda}\right) C\Big|_{intf} - \frac{C_s}{\tau} \tag{19}$$

where $D/\Lambda = \beta_{ad}$ is the kinetic constant for adsorption of solute from the solution at the interface into the adsorbed layer, with D being the bulk diffusivity, Λ is a characteristic length proportional to the resistance for adsorption, C_s is the surface (adsorption layer) solute concentration, and τ is the mean lifetime of an adsorbed molecule on the surface. Note that in contrast to the earlier model, where only steps formed sinks for the bulk transport, in the current model, as expressed by eq 19, all points on the interface represent potential sinks.

The conservation equation for the solute adsorbed on interstep terraces is

$$\frac{\partial C_s}{\partial t} = D_s \frac{\partial^2 C_s}{\partial x^2} + D \left.\frac{\partial C}{\partial z}\right|_{intf} \tag{20}$$

where the surface diffusivity D_s is assumed to be independent of the protein surface concentration. As in eq 19, the second term on the right-hand side of eq 20 represents the surface−volume exchange flux.

Following refs 136 and 137, it was assumed that the flux into a step, j_s, is proportional to the deviation of the surface concentration C_s at the step from its equilibrium value C_s^{eq}. On the ith terrace, bound by

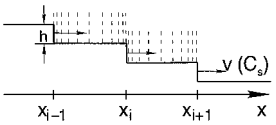

Figure 21. Steps in the interface with a one-dimensional surface diffusion grid and attached vertical grid lines of the domain. (Reprinted with permission from ref 205. Copyright 1999.)

the ith and $(i + 1)$th steps (located at $x = x_i$ and x_{i+1}, respectively), these fluxes are

$$j_s(x_i+) = D_s \left.\frac{\partial C_s}{\partial x}\right|_{x_{i+}} = \beta_s(C_s(x_i+) - C_s^{eq}) \quad (21a)$$

$$j_s(x_{i+1}-) = -D_s \left.\frac{\partial C_s}{\partial x}\right|_{x_{i+1}-} = \beta_s(C_s(x_{i+1}-) - C_s^{eq}) \quad (21b)$$

Here, β_s is the kinetic coefficient for incorporation of adsorbed molecules into steps and $-$ and $+$ denote, respectively, the terrace to the left and right of a step moving in the positive x direction, see Figure 21.

The bulk diffusion equation and eqs 19−21 represent the assumed pathway taken by the growth units from the solution into the crystal. It consists of bulk diffusion, followed by exchange of molecules between the adsorbed layer and the solution adjacent to the interface, diffusion of adsorbed molecules toward steps, and incorporation into steps, which results in step motion.

In all cases, equal kinetic coefficients were assumed for incorporation from the left terrace, β_s^-, and the right terrace, β_s^+, and express them in the form

$$\beta_s^- = \beta_s^+ = \beta_s = 0.5D_s/\Lambda_s \quad (22)$$

Here Λ_s is a characteristic length proportional to the resistance for incorporation from the surface into steps. Note that the restriction of eq 22 can be readily relaxed and the consequences of asymmetric kinetics of incorporation into steps[141] for step train stability can be studied without other changes in the model.

The characteristic surface diffusion velocity D_s/λ_s, see below, is on the order of 5 μm/s. This is an order of magnitude higher than the typical step velocity for lysozyme crystal growth of 0.5 μm/s. Hence, the neglect, in eq 20, of an advective contribution associated with step motion is well justified.

Furthermore, as in refs 83, 70, and 200, the steps were considered to be sufficiently rough, i.e., possess high kink density, so that diffusion along their edges can be ignored. Thus, the restriction of the model to two dimensions, with the steps represented as point sinks for the adsorbed solute, is also justified.

The surface flux into a step determines the step velocity according to

$$v = j_s\Omega/h \quad (23)$$

where $\Omega = 3 \times 10^{-20}$ cm^3 [43] is the volume per lysozyme molecule in the crystal and $h = 1.02 \times 10^{-6}$ cm is the step height.[72−75] Thus, accounting for the fluxes into a step from the left and right using eqs 21a,b, the velocity of the ith step at x_i can be expressed as

$$v_i = \frac{\Omega}{h}(j_s^- + j_s^+) = \frac{\Omega}{h}\{\beta_s[C_s(x_i-) - C_s^{eq}] + \beta_s[C_s(x_i+) - C_s^{eq}]\} \quad (24)$$

Steps that have a higher velocity will eventually catch up with slower ones. It was assumed that due to entropic repulsion between steps,[203,204] a pair of steps cannot form a double step or an overhang. Somewhat arbitrarily, the repulsive potential was chosen as a "hard sphere" interaction, with the characteristic distance between the steps set at five lattice parameters (=5h). The velocity of the trailing step in a pair that reached this critical separation is adjusted such that a closer approach is prevented.

The probability of step generation was evaluated as in section IV.C, however, using the surface rather than the bulk supersaturation as a driving force for the 2D nucleation.

For an equidistant step train at steady state and assuming that bulk transport is significantly faster than the interfacial processes, this model is equivalent to the one described in ref 136. Thus, the values of the kinetics constants for adsorption, desorption, surface diffusion, and incorporation into steps from the surface were extracted by correlating the experimentally determined $v(\sigma)$ to the theoretically derived dependencies in ref 136.

The "global" computational grid used for the diffusive bulk transport is identical to that used for the simulations reviewed in section IV.C.2, see Figure 18. As in that earlier work, the concentration distribution at the interface was obtained in a mesoscale grid that covers the narrow interfacial area. The horizontal grid spacing in the domain is based on a nonuniform one-dimensional surface grid used for the computation of C_s. This 1D grid is moved with the steps and is adjusted according to the changing widths of the terraces at each time step.

C. Stability with Respect to Small Perturbations

Evaluation of the model described in the previous subsection yielded excellent agreement with the results described in section IV.C and ref 205. Thus, both models reproduce the experimentally observed amplitudes and time scales of the fluctuations.

To investigate the effects of the magnitude of step density perturbations on the development of unsteady behavior, the frequency of generation of new growth steps at the facet edge was adjusted. In the case presented in Figure 22a, the resulting density of the newly generated steps was lower than the assumed initial density. This resulted in a cascade of step bunches spreading toward the facet center, very similar to those resulting from the earlier

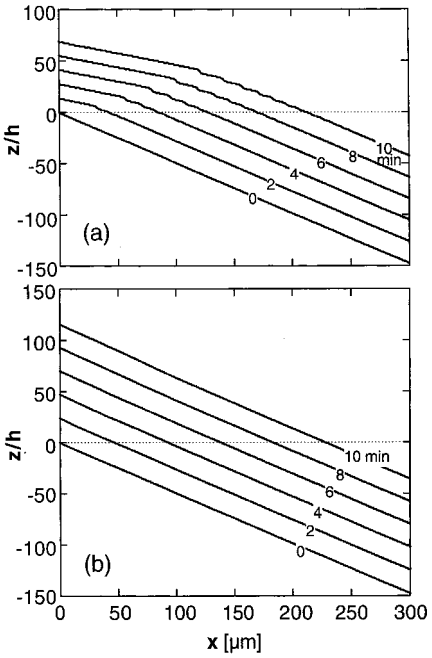

Figure 22. Interface profiles obtained at the simulation times indicated on the plots. *z*-values are in units of step height $h = 102$ Å. Changes in *z*-values at $x = 0$ account for layers generated between the times noted, i.e., individual steps remain at their *z* while propagating to the right. (a) Selected step generation frequency provides for a new slope lower than the initial assumption and cascade of step bunches obtains; (b) steps are generated with a frequency that ensures approximate preservation of the initial slope, no step bunches appear. (Reprinted with permission from ref 206. Copyright 1998 Elsevier Science.)

model.[185] Then the step nucleation frequency was increased until the new step density was roughly equal to the initial one. Figure 22b shows that no apparent step bunches are created, neither at the connection point between the old and new parts of the step train nor due to cascading.[206] Note that the correspondence between the new and the initial slope is only approximate, i.e., a small perturbation in the vicinal slope is still present even in the case depicted in Figure 22b. The lack of step bunches in this case indicates that whether a step density perturbation evolves into a step bunch with a continuously increasing slope will depend on the perturbation magnitude. This nonlinear response explains how groups of fewer dislocations (that produce more regular step sequences) may produce step trains that undergo significantly weaker bunching.

For a direct comparison with linear stability theories, see section IV.A, the preexponential coefficient in the nucleation rate equation was set to a value which ensures approximate preservation of the initial slope/step density on the crystal face even with decreasing supersaturation at the location of step generation. If a simulation is run with this value, no step bunching is observed despite the slight misfit between the initial and the newly developing slope. For the intended tests, after 5 min of growth via an equidistant step train, we imposed a 5% harmonic perturbation on step density by shifting each step by $\tilde{x}_i = 0.05(x_i - x_{i-1}) \sin(2\pi x_i/\hat{x})$, where x_i and x_{i-1} are the positions of the ith and $(i - 1)$th steps at 5 min and $\hat{x}$ is the perturbation wavelength. We chose three values of $\hat{x}$ (50, 100, and 200 μm) that cover the range of step bunching wavelengths observed in the experiments and simulations.

The results of these runs were output in terms of series of interfacial profiles and step density traces at three face locations. Both groups of results showed no step bunching for simulated growth times as long as an hour. This is not surprising: if perturbation with the form of a Heaviside step function, which is equivalent to a series of harmonic perturbations of various frequencies and amplitudes, does not cause step bunching, it is unlikely that a single harmonic perturbation may do so.

D. Experimental Evidence for the Role of Perturbation Type and Magnitude

Since small perturbations do not lead to step bunching and the consequent unsteady behavior recorded in the crystal growth experiments described in section III.A, it can be concluded that the observed kinetics fluctuations are triggered by large perturbations. Sufficiently large perturbations can be provided by irregular step generation (caused by random 2D nucleation or interaction between multiple dislocation sources, Figures 1 and 11) or by stoppers (adsorbed impurities, other dislocation outcrops, etc.) that lie in the path of a moving step (see section II.B.1, refs 124 and 205). This conclusion is supported by numerous observations of differences in fluctuation amplitudes and time scales for crystals with different growth step sources. For example, Figure 23 presents two fluctuation traces during the growth of the same crystal. The growth hillock shown in Figure 23b is steeper and, correspondingly, the average slope is higher. Note that this is associated with higher fluctuation amplitudes. The steeper slope reflects a step source of higher activity, likely due to cooperation of a larger number of dislocations than in Figure 23a. One can assume that the interactions between steps arising from a greater number of dislocations are more prone to delays, jumps, and other similar unsteadiness that, in turn, perturb the step train and cause the more significant fluctuations recorded for this case.

Further examples of correlations between changes in the activity of the dislocation growth step source and variations in unsteady behavior on the same crystal will be provided in section IX in the context of suspected effects on the average step kinetics.

These experimental and modeling results suggest that the step bunching associated with the growth kinetics fluctuations observed in experiments with the protein lysozyme are triggered by major step density variations. Such variations may arise from the intrinsically irregular nature of step generation by either two-dimensional nucleation or complex dislocation sources. Further irregularities in the step motion, and hence step density, may be introduced by various obstacles that impede the steps' progress: adsorbed impurity molecules or larger particles, points defects, dislocations outcrops, and other surface imperfections.

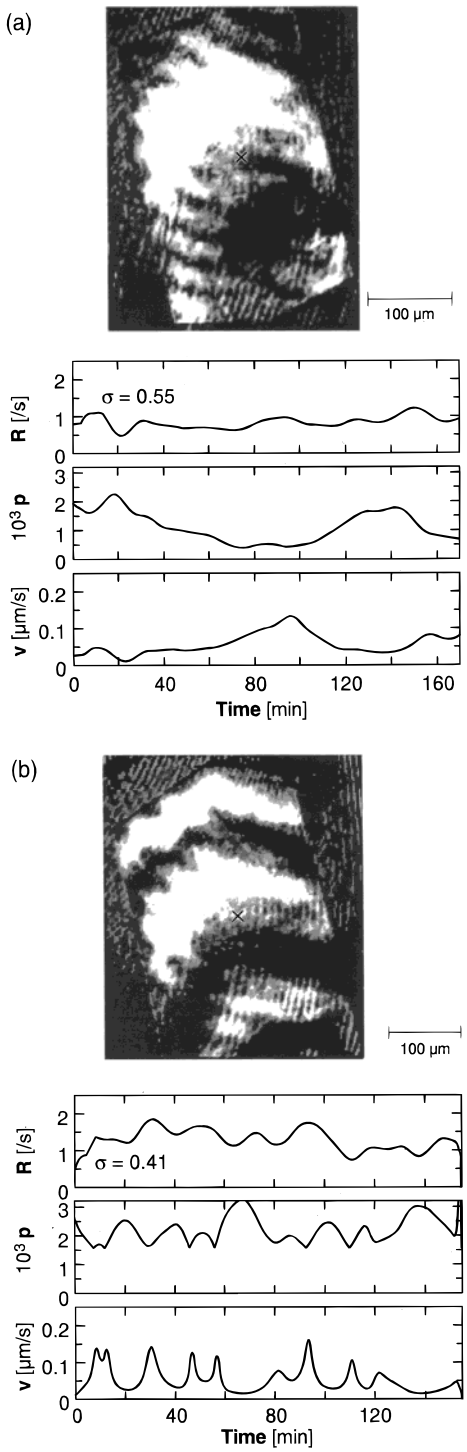

Figure 23. Time traces of normal growth rate R, local slope p, and tangential (step) velocity v obtained at the marked location (×) of the (110) facet shown in the interferograms. (a) Steps generated by dislocation bunch outcropping in lower part of facet. (b) Steps generated by dislocation bunch outcropping below bottom of interferogram. (Reprinted with permission from ref 163. Copyright 1996 American Physical Society.)

VI. Control of Kinetic Unsteadiness

In section IV, we showed that intrinsic kinetics fluctuations result in optically discernible defects that can compromise the crystals' utility for diffraction structure studies or for other purposes. Fortunately, based on the dependence of the amplitude of these fluctuations on the operating point (relative weight of transport and kinetics in overall rate control),[163] one can expect that shifts of the crystallization conditions toward either pure kinetics or transport control should result in more steady growth. Depending on the operating point of the specific system, such a shift toward more steady intrinsic conditions may require either enhanced (through forced convection) or damped (purely diffusive, as under reduced gravity) bulk transport. Note that lysozyme crystallization from unstirred solutions operates in a mixed regime with a dominant role of the interfacial kinetics in the overall rate control.[33,87,116,117] Thus, a reduction of the above step bunching instability should be expected for further shifts of the operating points to the right by enhancing the bulk transport. Tests of this rationale, i.e., the validity of the instability control parameter Pe_k, defined in eq 13 in section IV.C, were carried out through crystallization experiments in which the convection velocity was quantitatively varied.

For a given crystallization system, in principle, all three components of Pe_k can be varied. However, inducing variations in β_f (e.g., by changing the concentration of other solution components[208]) or D (by the addition of substances that increase viscosity[209,210]) may also lead to changes in the other two parameters. This introduces unaccountable variations in Pe_k. In flow parallel to the crystal−solution interface, the coupling between momentum and the concentration boundary layer results in the relation[211,212]

$$\delta = \kappa \left(\frac{D}{\nu}\right)^{1/3}\left(\frac{\nu x}{u}\right)^{1/2} \qquad (25)$$

where κ is a dimensionless parameter of ~5, ν is the kinematic viscosity of the solution, and x can be approximated by the crystal's linear dimension.

A. Experiments with Flowing Solution

Forced solution flow has been employed in protein crystallization experiments to replenish the solute consumed by the growing crystals and, thus, to obtain reproducible correlations between interfacial protein concentration and growth rates.[72,213] Furthermore, flow has been used to investigate the effects of solution convection on protein crystal growth.[115,214,215] The interest in convection was stimulated by the finding that with some proteins a reduction of buoyancy-driven convection in experiments conducted in low gravity resulted in improved crystal quality.[216−218] Hen egg-white lysozyme, particularly when purified by recrystallization, showed no difference in crystal growth rate and morphology whether grown in quiescent or flowing solutions.[72,219] In other studies in which the protein was used as supplied or after dialysis to remove small molecule components of the commercial powder, solution flow resulted in up to 20-fold growth rate reduction[115] or even complete growth cessation of tetragonal lysozyme.[214,215] Interestingly, the growth rate of rhombohedral lysozyme was not influenced by flow up to the same flow rates that caused cessation with the tetragonal form of the protein.[214] It has been suggested that the

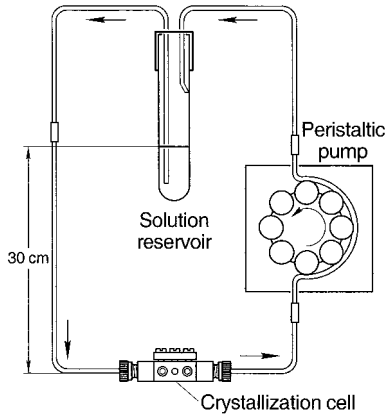

Figure 24. Schematic of solution circulation loop. Arrows indicate directions of solution flow. (Reprinted with permission from ref 221. Copyright 1998 Elsevier Science.)

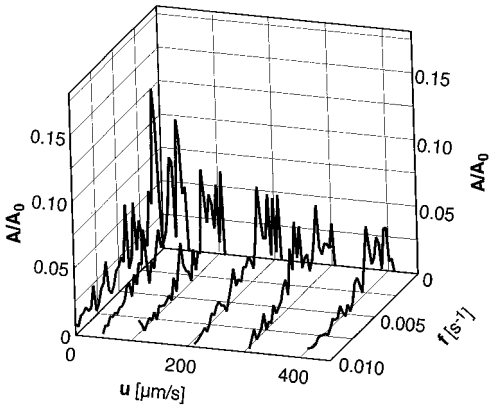

Figure 25. Normalized Fourier spectra $A(f)/A_0$ (f = Fourier frequency) of growth rate traces as a function of flow rate u during growth of a (101) face of a lysozyme crystal at $\sigma = 1.0$ ($T = 25$ °C) solution. (Reprinted with permission from ref 223. Copyright 1998 American Physical Society.)

growth impediment is the result of shear-induced conformational changes or even denaturation of the protein molecules by the flowing solution.[115] However, scaling analysis revealed that the shear forces on the length scale of a protein molecule, i.e., of O (50 Å), are several orders of magnitude lower than its thermal energy.[220] More recently it has been suggested that the growth deceleration in flowing solutions is due to incomplete mixing in the regions between multiple crystals.[215] Yet, this model has not been tested with experiments in which the number and density of crystallites in the crystallization cell was varied to change the solute supply conditions. More importantly, the incomplete mixing model obviously fails to explain the absence of flow effects observed for rhombohedral lysozyme.

A novel crystallization and solution circulation system, consisting of a crystallization cell, peristaltic pump, and reservoir, was developed for these investigations. As schematically indicated in Figure 24, the reservoir is placed at ~30 cm above the growth cell. The direction of solution flow is from the reservoir into the cell and on to the peristaltic pump. The jitter created by the pump is damped out when the solution re-enters the reservoir from the top and the solution is smoothly siphoned from the reservoir into the cell. The specific placement of the orifice of the return flow tubing in the reservoir with respect to the reservoir wall turned out to be crucial for avoiding protein denaturation. Close contact between this tubing and the reservoir wall ensured that the solution slowly slides down the reservoir wall and, thus, prevented denaturation. This system allows solution flow through the cell with velocities (measured at distances of a few crystal dimensions form the crystal) that can be varied in the range from 20 μm/s, comparable to the buoyancy-driven convection velocities, up to 2000 μm/s to amplify possible convection effects. Further details on the design and extensive tests performed with this setup are provided in ref 221.

B. Suppression of Unsteadiness with Faster Bulk Transport

In the experiments reviewed here, the flow velocity u was essentially in the direction of step motion and varied between 40 and 420 μm/s. Thus, with $\nu = 1.32 \times 10^{-2}$ cm^2/s[220] and $x = 100$ μm, according to eq 25, δ was varied between 350 μm and 105 μm. With the lysozyme parameters $\beta_f = 10^{-6}$ cm/s[87] and $D = 7 \times 10^{-7}$ cm^2/s,[24] the corresponding Pe_k's range from 0.050 to 0.015. In the absence of forced flow, buoyancy-driven convection leads to $\delta \approx 300$ μm,[88,115] resulting in $Pe_k \approx 0.05$. Thus, the above range in flow velocity should reveal the effects of shifting the system from its operating point in unstirred solutions to a regime with significantly faster transport and higher relative weight of interfacial kinetics in the overall process control.

Figure 25 shows Fourier spectra normalized with respect to $A_0 = R_{avg}$ for several flow velocities throughout the investigated range. We see that the fluctuation amplitudes monotonically decrease with increasing flow velocity. These observations were interpreted, according to eqs 13 and 25 from sections IV.C.1 and VI, in terms of decreasing δ with increasing u. The higher transport rates reduce Pe_k and, thus, stabilize the growth kinetics.

Trends identical to those represented by Figure 25 were recorded with numerous crystals[223,224] at supersaturations σ ranging from 0.58 to 1.8, using solutions of different purity. This confirms transport enhancement as a means of shifting the operating point of the system from the mixed regime toward kinetics control, thereby suppressing the fluctuation amplitudes and increasing the stability of the growth process against rate/flux perturbations. Note also that these effects are different from the previously observed reduction of step bunching by forced solution flow[195] that was analyzed in terms of linear stability.[196,198] For the latter, stabilization occurred only with flows opposite to the step motion direction. However, the results for the lysozyme system, reviewed here and in other related papers,[223,224] do not depend on the relative directions of step motion and solution flow, including essentially parallel motion of steps and solution. Further indication of the inapplicability of these linear stability analyses to the observations in refs 163 and 169 was discussed in section V.A in relation to the observation that step

bunch wavelengths lie within the predicted region of stability for equidistant step trains (see section V.A).

VII. Impurities and Kinetic Unsteadiness

Impurities with a molecular size larger than that of the basic protein or 3D nuclei,[78,79,225,226] due to their lower diffusivity, are more depleted in the interfacial region than the host protein itself.[227,228] Thus, in the absence of convective transport, the incorporation of potentially defect-inducing large impurities, aggregates, and nuclei into a crystal may be significantly reduced. To test how convective transport influences the impurity-induced kinetics effects, we compare in Figure 26 the flow rate dependencies of the Fourier spectra, characteristic of the unsteady kinetics. These dependencies were recorded during the growth from ultrapure lysozyme solutions[56] and solutions intentionally contaminated with 1% lysozyme dimer, produced and isolated as described in ref 229. Such impurity levels are commensurate with those typical in protein crystallization solutions. All kinetics data were obtained during the growth of one crystal, and the interferometric images revealed that the growth layer source was located at the lower facet corner throughout the measurements. For further details, see ref 224.

We see in Figure 26a that after the initial decrease in fluctuation amplitudes up to flow rates of ~500 μm/s, the amplitudes again increase and reach values even higher than in unstirred solutions. During growth from the less pure solution, Figure 26b, the fluctuation amplitude starts increasing at about one-half the flow rate at which this increase is observed

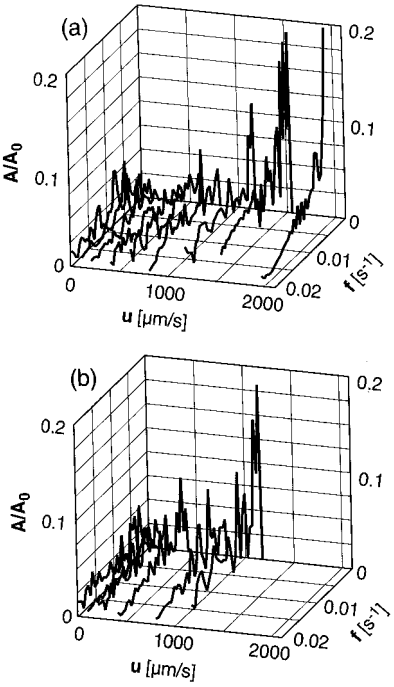

Figure 26. Normalized Fourier spectra $A(f)/A_0$ (f = Fourier frequency) of growth rate traces obtained at $\sigma = 1.4$ (T = 22 °C) as a function of flow rate u during growth from solutions before (a) and after (b) the addition of ~1% lysozyme dimer to 99.99% pure lysozyme. (Reprinted with permission from ref 224. Copyright 1997 American Chemical Society.)

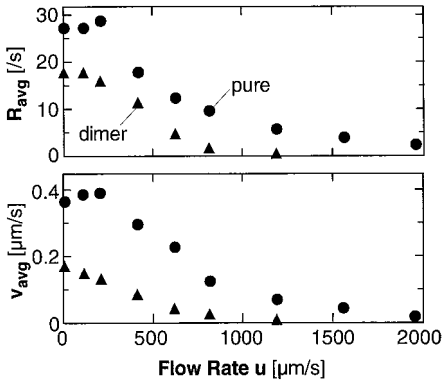

Figure 27. Flow rate dependence of the average growth rate R_{avg} and step velocity v_{avg} at two solution purity levels at $\sigma = 1.4$ (T = 22 °C), corresponding to the traces whose Fourier spectra are displayed in Figure 26. (Reprinted with permission from ref 224. Copyright 1998 American Chemical Society.)

in the pure solutions. Figure 27 shows the dependencies of the averaged growth rate and step velocity on the flow rate for the pure and contaminated solutions, corresponding to the growth regimes characterized by the Fourier spectra in Figure 26. In the intentionally contaminated solution, R_{avg} and v_{avg} decrease with increasing u even at the lowest flow rates. Growth ceases at $u \approx 1000$ μm/s, while in the pure solution, growth initially accelerates with increasing flow rate, reaches a maximum R_{avg} at $u \approx 450$ μm/s, and retains significant, albeit reduced magnitudes at all flow rates studied. When similar tests are carried out at lower supersaturation, e.g., $\sigma = 1.0$, growth cessation is reached at $u \approx 1500$ μm/s even in the high-purity solution. This is related to the longer exposure times of the interstep terraces to impurity adsorption at the lower R's typical for such values of σ.[71,87]

The amplification of the decrease in magnitude of R and v at higher $u-$ velocities and higher lysozyme dimer concentrations indicates that this is due to flow-enhanced transport of the growth-inhibiting impurity to the interface. This mechanism requires that the impurity amount per unit volume in the crystal is higher than that in the solution and that its diffusivity is sufficiently low such that the impurity concentration at the interface is lower than that in the bulk solution. Only then can enhanced, convective transport increase the interfacial impurity concentration.

To test for the impurity repartitioning, lysozyme crystals were grown from solutions prepared from Seikagaku lysozyme, which contains about 1% of other protein impurities.[56] The solution was divided into samples of 0.5 mL in sealed tubes. Pairs of tubes were kept for 15 days at 20 °C, i.e., at a temperature representative of the growth kinetics studies. A control tube the was kept at room temperature, 25−27 °C, and no crystals formed in it. For analysis, the supernatant was separated from the crystals by careful decanting into an empty tube and the crystals were twice rinsed with water chilled to 0 °C.[148] Then the crystals were dissolved in 0.5 mL of acetate buffer, and the protein concentration of the supernatant and dissolved crystals was determined by

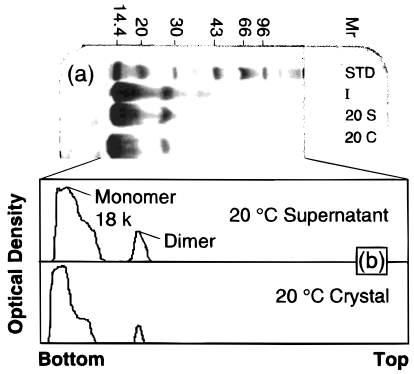

Figure 28. Analysis of impurity repartitioning upon crystallization by electrophoresis. (a) SDS PAGE 12.5% homogeneous Pharmacia PhastGel with silver staining. The solution was concentrated or diluted to bring the protein concentration to 10 mg/mL in each sample, with 0.3 μL loaded in each lane: lane 1, standards; lane 2, initial solution control; lane 3, supernatant after separation from the crystals; lane 4, dissolved crystals. (b) Optical density scans of lanes 3 and 4 in part a. (Reprinted with permission from ref 206. Copyright 1998 Elsevier Science.)

SDS−PAGE.[56] Since each gel lane was loaded with the same solution volume, differences of impurity band intensities are representative of the differences of the impurity amounts per lysozyme molecule in the samples.

The gels are shown in Figure 28. It is seen that the dimer with MW ~29 000 is indeed incorporated into the crystals. Taking into account the change of monomer density upon crystallization, ~16 times, the gels show that the amount of dimer per unit volume in the crystals is about 5 times higher than in the solution. In addition, it is safe to assume that the larger dimer has a lower diffusivity in the solution than the monomer.

These observations strongly support the proposed mechanism for convective flow increase of the amplitude of defect-causing fluctuations due to enhanced impurity to the interface. Although the flow velocities at which these effects were observed were significantly higher than buoyancy-driven convection velocities, note that the purity of the material used is also significantly higher than normally employed in protein crystallization practice. Thus, it is conceivable that with solution purity on the order of 95−99%, such impurity-induced instabilities and striations may occur at the flow velocities typical of buoyancy-driven convection.

VIII. Rationale for System-Dependent Effects of Bulk-Transport Changes on Crystal Perfection

On the basis of the above findings, we can speculate how changes in the transport conditions may affect the quality of the protein crystals or other systems with mixed transport−kinetics control. If, for instance, for the growth of a certain (protein) material on Earth bulk-transport and interfacial kinetics have comparable weights in the overall rate control, fluctuation amplitudes may be significant. In this case, a shift of the operating point toward higher kinetics control due to slower transport in the absence of buoyancy-driven convection under low-gravity conditions can dampen the fluctuations. This can result in higher crystal perfection. On the other hand, crystallization systems with slower surface kinetics and faster transport would operate under stronger transport control. Then on suppression of convective transport in space, fluctuation amplitudes may increase and the crystal quality decrease. Furthermore, in some case the reduced supply of impurities to the growth interface in space may also contribute to higher crystal perfection. Similar considerations may help us rationalize why only about 20% of the proteins and viruses that were crystallized under reduced gravity yielded higher X-ray diffraction resolution than their controls grown on Earth.[230] The remainder either showed no improvement or diffracted to lower resolution either due to smaller sizes or, as documented for a few cases, lower crystal perfection.[231,232]

Table 1. Estimated Kinetic Peclet Numbers of Lysozyme, Thaumatin, Canavalin, and Satellite Tobacco Mosaic Virus (STMV) Using a Characteristic Diffusion Length $\delta = 300$ μm.[199] For Sources of Data, See Text

	lysozyme	thaumatin	canavalin	STMV
D [10^{-6} cm^2/s]	0.73	0.6	0.4	0.2
$\beta_f = \beta_{step}p$ [cm/s]	1×10^{-6}	2×10^{-6}	5×10^{-6}	8×10^{-6}
$Pe_k = \beta_f\delta/D$	0.05	0.1	0.38	1.2

A. Pure Solutions

It is useful to test the above rationale by analyzing its predictions for the results of actual protein crystal growth experiments carried out in microgravity. Note that the discussion in this subsection only concerns pure protein solutions. Implications for protein crystal quality from the changes in supply rates of impurities to the interface will be reviewed in the next subsection. Some general recommendations for pure and impure protein solutions will be provided at the end of the section.

In section IV.A, we characterized the relative importance of transport and interface processes by the kinetic Peclet number. This Pe_k was evaluated for four proteins that were crystallized both on Earth and under reduced gravity and for which the kinetic coefficients, see section II.B.1, as well as the diffusivities are known,[24,26,233] see Table 1.[234]

For lysozyme and thaumatin, Pe_k values reflect kinetics-dominated growth. For lysozyme, this is expected from earlier studies.[33,88,116,117,123] Hence, from the point of view of nonlinear response, an increase of bulk-transport contributions to growth rate control under reduced gravity should not result in increased structural perfection, i.e., little or no improvements from microgravity growth should be expected. This corresponds to the results for space-grown lysozyme.[232] Exceptions to this that were observed in earlier tests with lysozyme[235] and thaumatin[236] may be due to reduced impurity supply in the absence of convection in space, see below and refs 223 and 237, and/or the lack of sedimentation.[230]

For canavalin and STMV, the Pe_k's indicate that these systems operate on Earth more in the mixed-control regime. Furthermore, space-grown canavalin

and satellite tobacco mosaic virus (STMV) crystals yielded higher diffraction resolution.[227,228] This suggests that the higher perfection of space-grown crystals of these materials could be due to a reduction in nonlinear response, i.e., a shift of the working point toward transport control resulting from the diffusive transport at low gravity.

Besides the possible damping of growth rate fluctuations, there are other benefits from the reduced-gravity conditions. For example, sedimentation of foreign particles or microcrystals on a growing facet is dramatically reduced.[230] However, the argument outlined above provides a *system-dependent* rationale for advantages *as well as disadvantages* of reduced-gravity growth conditions for (protein) crystal perfection.

B. Impure Proteins

The effects of enhanced impurity transport on step bunching, discussed in section VII, may underlie observed improvements in the quality of lysozyme[235] and thaumatin[236] crystals grown in microgravity. In both studies, the crystals were grown from material as received from Sigma, without any further purification. Lysozyme batches from Sigma have been shown to contain as much as 5% of larger proteins,[56] while the thaumatin material, according to the manufacturer, is a mixture of mainly two protein species with traces of other sweet proteins.

Thus, if impurities are responsible for crystal quality degradation, a microgravity environment, by minimizing such flows, can result in substantial improvements. This conclusion is supported by recent results on lysozyme crystals grown in the absence of buoyancy-driven convection in microgravity from a low-purity solution, which showed lower impurity incorporation *and* higher diffraction resolution than identically grown Earth controls.[237]

These results are also relevant to the growth cessation at a "terminal crystal size" often observed by practitioners. At larger crystal sizes, the velocities of buoyancy-driven flows are higher.[174] This enhances the impurity supply to the interface, which, in turn, causes "surface poisoning" and growth cessation. Furthermore, this mechanism may also be responsible for the larger crystal sizes obtained in some microgravity growth runs.[10,218,236] So far, such observations have resisted explanation since decelerated solute transport in space should cause reduced interfacial supersaturation, slower growth, and, hence, for the limited duration of a space flight smaller crystals.

C. What Should We Do before Conducting Low-Gravity Experiments?

From the rationales for pure and impure solutions reviewed in the above two subsections, a few steps can be taken to optimize the yield of the expensive protein crystal growth experiments in space. First, one would recommend state-of-the-art characterization and purification of the protein material by using conditions (pH, ionic strength, type and concentration of accompanying salt and other additives) that have been specifically found to produce the highest separations from the impurities typical for the material of interest. If this approach is carried out consistently, so-called microgravity filtering of impurities by decelerating their access to the interface may be unnecessary. When this approach was recently applied to the pair ferritin/apoferritin, it yielded ~1 Å improvement in diffraction resolution even in Earth-grown crystals.[84] Of course, for some extremely scarce proteins, there is insufficient material to develop and optimize comprehensive purification procedure. Other proteins may not be readily purified using currently available techniques. In these cases, it may be worth purifying the interfacial solution layer under microgravity conditions to achieve lower impurity supply and, hence, higher crystal perfection.

Second, even if high-purity protocols exist for a protein of interest, microgravity benefits can be expected if the kinetic Peclet number indicates mixed or transport-controlled growth regimes on Earth. For such materials, the effective reduction of the transport rates in the absence of buoyancy-driven convection will eliminate kinetics fluctuations and lead to higher crystal perfection. To be able to unambiguously predict benefits from the growth of crystals under reduced gravity, the transport and kinetic properties of the crystallizing system would have to be studied. Such investigations may take several months, but they will definitely occupy less time and resources than a space-flight experiment that does not yield crystals of better quality than what can be achieved under terrestrial conditions.

IX. Does Step Bunching Contribute to the Slow Protein Crystal Growth?

Some of the growth runs with lysozyme that were monitored using interferometry yielded growth rate R and step velocity v values significantly higher than in any previous measurements regardless of the material purity. In some cases, these values were also higher than those obtained at earlier stages of growth of the same crystal, during which the crystal was smaller and the growth layers were generated by other dislocation step sources. An example of such kinetics results is given in Figure 29 together with typical lower R_{avg} and v_{avg} values obtained on the smaller crystal. Corresponding growth morphologies are shown in Figure 30a,b.

The $v_{avg}(\sigma)$ dependence in Figure 29b is well reproduced by the relation

$$v_{avg} = \frac{\beta\Omega C_{eq}(C/C_{eq} - 1)}{1 + kp_{avg}} \qquad (26)$$

where Ω is the molecular volume in the crystal, with the step kinetic coefficient $\beta_{st} = 2 \times 10^{-3}$ cm/s and step field overlap parameter $k = 500$. This is shown by the curve calculated from eq 26 with these parameters and the $p_{avg}(\sigma)$ dependence recorded in parallel with R_{avg} and v_{avg}. The value of k agrees well with previous determinations for the same system (see discussion in section II.B.2). However, the value of β_{st} is about 10−50 times higher than previously determined, see section II.B.1.

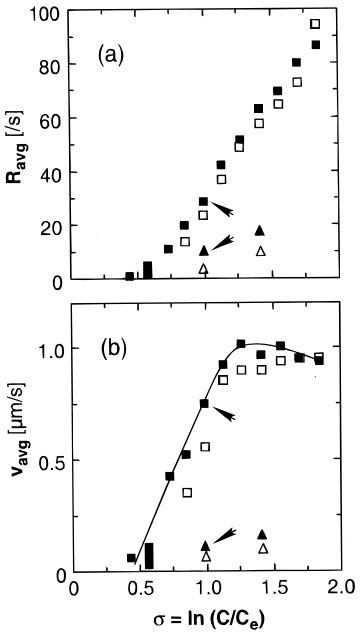

Figure 29. Supersaturation dependence of the normal growth rate R (a) and step velocity V (b) averaged over periods on the order of 1 h. Growth from solution containing 1% lysozyme dimer: (■, ▲) $u = 105$ μm/s; (□, △) $u = 305$ μm/s; (■, □) series of measurements at the end of run, representative growth morphology is shown in Figure 30b; (▲, △) measurements at earlier stages of growth of the same crystal, representative growth morphology is shown in Figure 30a. Curve in part b presents data fit to ■ according to eq 26, for parameters see text. Arrows indicate conditions for which the fluctuation characteristics are displayed in Figure 30c,d. (Reprinted with permission from ref 224. Copyright 1998 American Chemical Society.)

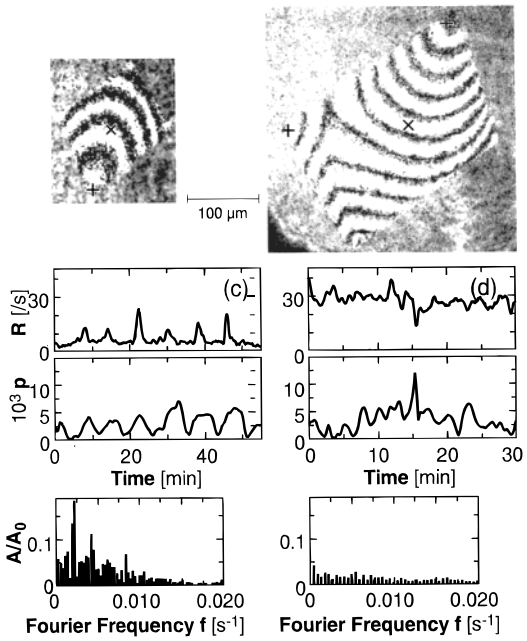

Figure 30. (a,b) Representative morphologies of the facet during the recording of the kinetic data presented in Figure 5: (+) location of layer generation; (×) location of growth kinetics monitoring. (c,d) Traces of normal growth rate R, vicinal slope p, and Fourier spectra of R corresponding to the points marked by arrows in Figure 29 at $\sigma = 1.0$ ($T = 25$ °C) and $u = 105$ μm/s. Small crystal size in part a corresponds to stronger fluctuations in part c and lower step velocity and growth rate in Figure 29. (Reprinted with permission from ref 224. Copyright 1998 American Chemical Society.)

To rationalize this high β_{st} value at the larger crystal size (compare parts a and b in Figure 30), recall that as a crystal grows, the dislocation source activity drops, see section II.A.3. This decrease was related to diverging lines of bunched dislocations, leading to fewer dislocations within a distance ρ_c corresponding to the radius of a critical 2D nucleus where they act as a joint growth layer source. Furthermore, as discussed in connection with the numerical simulations of step bunching in sections IV.C and V and in refs 185 and 205, unsteadiness in step source activity acts as a trigger for the bunching that underlies the growth rate fluctuations. As the number of dislocations in a growth layer source decreases with crystal size, it is reasonable to expect that the layer generation becomes more regular and the step density perturbations weaken. This results in reduced step bunching in the generated step train. It appears that such a step train spreads with higher v_{avg} than a step train with higher step bunches.

This hypothesis is supported by Figure 30c,d, which presents the fluctuation patterns corresponding to the pair of R and v measurements at $u = 105$ μm/s and $\sigma = 1.0$, marked by arrows in Figure 29. We see that a faster growth rate and step velocity are associated with lower step bunching and growth rate fluctuations. An analogy can be found between certain traffic flow situations and the correlation between the higher average step velocity and more uniform step spacing. Consider a certain section of the road where the distance between cars is constant. The residence time of each car in this section will be shorter than the residence time in an equivalent length section where there are traffic jams even if the overall number of cars in this section, i.e., the average car density, is the same. A more rigorous theoretical discussion of the relation between this of type step bunching and averaged step velocity will be presented elsewhere.[238]

Numerous additional experiments with lysozyme revealed similar correlations between the fluctuation amplitudes and v_{avg}. The highest value of the kinetic coefficient, found in these studies by substituting the average values for p and v into eq 26, was 4.1×10^{-3} cm/s. Such high β_{st} values are comparable to the step kinetic coefficient for some inorganic crystal growth systems[239−241] and exceed all published kinetic coefficients for proteins, section II.B.1, by 1−2 orders of magnitude. This suggests that some interpretations of the small values of the protein kinetic coefficients[106] may need to be revisited.

Besides the effects of step bunching on average growth rate in pure systems, step bunching may result in enhanced impurity effects. Thus far, impurity effects on growth have only been discussed in terms of the retardation of individual steps in equidistant step trains.[120−122,125,126] However, impurities are also known to cause step bunching.[242,243] Hence, in view of the above scenario, growth deceleration due to impurities can be strongly amplified by the interaction of steps in trains that have become nonuniform due to impurity action. Such a synergistic mechanism may underlie, for instance, the unusual dependence

of the "dead-zone" width on the bulk concentration of impurities observed in a recent study of KDP crystal growth.[244] This strong dependence exceeds, by far, the predictions even of most comprehensive models of impurity action based on trains of equidistant steps.[120−122]

Another consequence of the correlation between growth step bunching and growth rate is that it provides a novel mechanism for temperature effects on the growth rate. If the step patterns depend on temperature, this dependence should be accounted for in determinations of the activation barriers of the constituent steps of the crystal growth mechanisms. Furthermore, since bunching also depends on the growth layer source, which varies from crystal to crystal, weaker or stronger temperature dependencies of the growth rate are possible for different crystals. Experimental evidence in support of this temperature dependence can be found in refs 128 and 129 in which interferometry was used to characterize surface features and determine v_{avg} and β. The effective activation energy for growth step propagation was found to be higher by about 20 kJ/mol at lower temperatures. This value was attributed to the additional growth step acceleration due to weaker bunching with increasing temperature.

X. Concluding Remarks

Besides the significance for the quality of the protein crystals, the unsteady dynamics of layer growth discussed above may have numerous other implications. It is a fascinating model for unsteady processes that occur not only during phase transitions in crystal growth or other areas of materials science,[245] but also in many branches of physics, in various biological systems,[246] that may have long-ranging medical consequences.[247]

Questions that need to be addressed in all such studies concern the character of the unsteady behavior. Is it a deviation from the normal steady behavior of the system or is unsteadiness the norm and steady-state nonexistent?

Specific questions related to protein crystallization involve the particular character of the unsteady phenomena during growth of other protein crystals and under a broader variety of conditions: forced flow, full suppression of convection under microgravity, etc.

XI. Acknowledgments

We are deeply indebted to our collaborators who have contributed to some of the original studies reviewed here: F. Rosenberger, H. Lin, and B. R. Thomas. We also thank S.-T. Yau and S. Weinkauf for making some unpublished results available, A. A. Chernov and D. C. Carter for stimulating discussions on various aspects of this work, and A. J. Malkin for important references. L. Carver expertly prepared the figures. This work was supported by the Life and Microgravity Science and Applications Division of NASA, by the National Heart, Blood and Lung Institute, NIH, and by the State of Alabama through the Center for Microgravity and Materials Research at the University of Alabama—Huntsville and the Alabama Supercomputer Network.

XII. References

(1) Darby N. J.; Creighton, T. E. *Protein Structure*; Oxford University Press: Oxford, 1993.
(2) Glaser, S. J.; Schulte-Herbrüggen, T.; Sieveking, M.; Schedletzky, O.; Nielsen, N. C.; Sørensen, O. W.; Griesinger, C. *Science* **1998**, *280*, 421.
(3) Chayen, N. E.; Boggon, T. J.; Casseta, A.; Deacon, A.; Gleichmann, T.; Habash, J.; Harrop, S. J.; Helliwell, J. R.; Neih, Y. P.; Peterson, M. R.; Raftery, J.; Snell, E. H.; Hädener, A.; Niemann, A. C.; Siddons, D. P.; Stojanoff, V.; Thompson, A. W.; Ursby, T.; Wulff, T. M. *Q. Rev. Biophys.* **1996**, *29*, 227.
(4) DeLucas, L.J; Bugg, C. E. *Trends Biotechnol.* **1987,** *5*, 188.
(5) Weber, P. In *Advances in Protein Chemistry*; Afinsen, C. B., Richards, F. M., Edsal, T. J., Eisenberg, D. S., Eds.; Academic Press: New York, 1991; Vol. 41.
(6) Matsuda, S.; Senda, T.; Itoh, S.; Kawano, G.; Mizuno, H.; Mitsui, Y. *J. Biol. Chem.* **1989,** *264*, 13381.
(7) Peseta, S.; Langer, J. A.; Zoon, K. C.; Samuel, C. E. In *Annual Review of Biochemistry*; Richardson, C. C., Boyer, P. D., Dawid, I. B., Meister, A., Eds.; Annual Reviews: Palo Alto, 1989; Vol. 56, p 727.
(8) Brange, J. *Galenics of Insulin*; Springer: Berlin, 1987.
(9) Reichert, P.; McNemar, C.; Nagabhushan, N.; Nagabhushan, T. L.; Tindal, S.; Hruza, A. Metal-interferon-alpha crystals. U.S. Patent No. 5,441,734, 1995.
(10) Long, M. L.; Bishop, J. B.; Nagabhushan, T. L.; Reichert, P.; Smith, G. D.; DeLucas, L. J. *J. Cryst. Growth* **1996**, *168*, 233.
(11) Charache, S.; Locksard-Conley, C. L.; Waugh, D. F.; Ugoretz, R. J.; Spurrell, J. R. *J. Clin. Invest.* **1967**, *46*, 1795.
(12) Hirsch, R. E.; Raventos-Suarez, C.; Olson, J. A.; Nagel, R. L. *Blood* **1985,** *66*, 775.
(13) Ferrone, F. A.; Hofrichter, J.; Eaton, W. A. *J. Mol. Biol.* **1985**, *183*, 591. Ferrone, F. A.; Hofrichter, J.; Eaton, W. A. *J. Mol. Biol.* **1985**, *183*, 611.
(14) Berland, C. R.; Thurston, G. M.; Kondo, M.; Broide, M. L.; Pande, J.; Ogun, O.; Benedek, G. *Proc. Natl. Acad. Sci. U.S.A.* **1992**, *89*, 1214.
(15) Rosenberger, F. *Cryst. Res. Technol.* **1999**, *34*, 163−165.
(16) Oxtoby, D. W. *J. Phys.: Condens. Matter* **1992**, *4*, 7627−7650.
(17) Melnik, O.; Sparks, R. S. J. *Nature* **1999**, *402*, 37−41.
(18) Ren, H.-W.; Shen, X. Q.; Nishinaga, T. *J. Cryst. Growth* **1995**, *166*, 217−221.
(19) Pusey, P. N.; van Megen, W. *Nature* **1986**, *320*, 340.
(20) Van Mewgen, W.; Underwood, S. M. *Nature* **1993**, *362*, 616.
(21) Harland, J. L.; Henderson, S. J.; Underwood, S. M.; van Megen, W. *Phys. Rev. Lett.* **1995**, *75*, 3572.
(22) Kam, Z.; Shore, H. B.; Feher, G. *J. Mol. Biol.* **1978**, *123*, 539.
(23) George, A.; Wilson, W. W. *Acta Crystallogr., Sect. D* **1994**, *50*, 361.
(24) Muschol, M.; Rosenberger, F. *J. Chem. Phys.* **1995**, *103*, 10424.
(25) Rosenberger, F.; Vekilov, P. G.; Muschol M.; Thomas, B. R. *J. Cryst. Growth* **1996**, *168*, 1.
(26) Malkin, A. J.; McPherson, A. *Acta Crystallogr., Sect. D* **1994**, *50*, 385.
(27) Rosenberger, F. *J. Cryst. Growth* **1986**, *76*, 618.
(28) Baird, J. K.; Meehan, Jr., E. J.; Xidis, A. L.; Howard, S. B. *J. Cryst. Growth* **1986**, *76*, 694.
(29) Ramachandran, N.; Baugher C. R.; Naumann, R. J. *Microgravity Sci. Technol.* **1995**, *8*, 170.
(30) Gratz, A. J.; Manne, S.; Hansma, P. K. *Science* **1991**, *251*, 1343.
(31) Hillner, P. E.; Manne, S.; Hansma, P. K.; Gratz, A. J. *Faraday Discuss.* **1993**, *95*, 191.
(32) Vekilov, P. G.; Ataka, M.; Katsura, T. *J. Cryst. Growth* **1993**, *130*, 317.
(33) Vekilov, P. G. In *Studies and Concepts in Crystal Growth*; Komatsu, H., Ed.; Pergamon Press: Oxford, 1993; p 25.
(34) Vekilov, P. G.; Monaco, L. A.; Rosenberger, F. *J. Cryst. Growth* **1995**, *146*, 289.
(35) Kuznetsov, Yu. G.; Malkin,.A. J.; Greenwood, A.; McPherson, A. *J. Struct. Biol.* **1995**, *114*, 184.
(36) Kuznetsov, Yu. G.; Malkin, A. J.; Greenwood, A.; McPherson, A. *J. Cryst. Growth* **1996**, *166*, 913.
(37) Malkin, A. J.; Land, T. A.; Kuznetsov, Yu. G.; McPherson, A.; DeYoreo, J. J. *Phys. Rev. Lett.* **1996**, *75*, 2778.
(38) Land, T. A.; Malkin, A. J.; Kuznetsov, Yu. G.; McPherson, A.; DeYoreo, J. J. *Phys. Rev. Lett.* **1996**, *75*, 2774.
(39) Yip, C. M.; Ward, M. D. *Biophys. J.* **1996**, *71*, 1071.
(40) Feigelson, R. S. *J. Cryst. Growth***1988**, *90*, 1.
(41) Boistelle, R.; Astier, J. P. *J. Cryst. Growth* **1988**, *90*, 14.
(42) Blake, C. C. F.; Johnson, L. N.; Mair, G. A.; North, A. C. T.; Phillips, D. C.; Sarma, V. R. *Proc. R. Soc. London, Ser. B.* **1967,** *167*, 378.
(43) Steinrauf, L. K *Acta Crystallogr.* **1959**, *12*, 77.

(44) Blake, C. C. F.; Koenig, D. F.; Mair, G. A.; North, A. C. T.; Phillips, D. C.; Sarma, V. R. *Nature* **1965,** *206*, 757.
(45) Blake, C. C. F.; Mair, G. A.; North, A. C. T.; Phillips, D. C.; Sarma, V. R. *Proc. R. Soc. London, Ser. B.* **1967,** *167*, 365.
(46) Rariy, R. V.; Klibanov, A. M. *Proc. Natl. Acad. Sci. U.S.A.* **1997**, *94*, 13520−13523.
(47) Broide, M. L.; Tominc, T. M.; Saxowski M. D. *Phys. Rev. E* **1996**, *53*, 6325.
(48) Velev, O. D.; Kaler, E. W.; Lenhoff, A. M. *Biophys. J.* **1998**, *75*, 2682.
(49) Mutaftschiev, B. In *Handbook of Crystal Growth. 1. Fundamentals. Part A: Thermodynamics and Kinetics*; Hurle, D. T. J., Ed.; North-Holland: Amsterdam, 1993; p 187.
(50) Kashchiev, D. In *Science and Technology of Crystal Growth*; van der Eerden, J. P., Bruinsma, O. S. L., Ed.; Kluwer: Academic Publishers: Dordrecht, 1995; p 53.
(51) Higo, J.; Nagayama, K. *J. Phys. Chem.* **1993**, *99*, 9156.
(52) Frey, W.; Schief, W. R., Jr.; Vogel, V. *Langmuir* **1996**, *12*, 1312.
(53) Frey, W.; Schief, W. R., Jr.; Pack, D. W.; Chen, C.-T.; Chilkoti, A.; Stayton, P.; Vogel, V.; Arnold, F. H. *Proc. Natl. Acad. Sci. U.S.A.* **1996**, *93*, 4937.
(54) McPherson, A. *Preparation and Analysis of Protein Crystals*; Wiley: New York, 1982.
(55) *Crystallization of Nucleic Acids and Proteins: A Practical Approach;* Ducruix, A., Giege, R., Eds.; IRL Press: Oxford, 1992.
(56) Thomas, B. R.; Vekilov, P. G.; Rosenberger, F. *Acta Crystallogr., Sect. D* **1996,** *52*, 776.
(57) Retailleau, P.; Ries-Kaut, M.; Ducruix, A. *Biophys. J.* **1997**, *73*, 2156.
(58) Stranski, I. N.; Kaischew, R. *Z. Phys. Chem. B* **1934**, *26*, 100.
(59) Kaischew, R.; Stranski, I. N. *Z. Phys. Chem. B* **1934**, *26*, 114.
(60) Stranski, I. N.; Kaischew, R. *Z. Phys. Chem. B* **1934**, *26*, 312.
(61) Jackson, K. A. In *Growth and Perfection of Crystals*; Doremus, R. H., Roberts, B. W., Turnbull, D., Eds.; Chapman and Hill: London, 1958.
(62) Gilmer, G. H In *Handbook of Crystal Growth*; Hurle, D., Ed.; North-Holland: Amsterdam, 1994; Vol. 1a, p 583.
(63) Van der Eerden, J. P. In *Handbook of Crystal Growth*; Hurle, D., Ed.; North-Holland: Amsterdam, 1994; Vol. 1a, p 307.
(64) Burton, W. K.; Cabrera, N. *Discuss. Faraday Soc.* **1949**, *5*, 33.
(65) Volmer, M. *Z. Phys. Chem.* **1922**, *102*, 267.
(66) Stranski, I. N. *Z. Phys. Chem.* **1928**, *136*, 259.
(67) Kaischew, R.; Budevski, E. *Contemp. Phys.* **1967**, *8*, 489.
(68) Milchev, A. *Contemp. Phys.* **1991**, *32*, 321.
(69) Frank, F. C. *Discuss. Faraday Soc.* **1949**, *5*, 48.
(70) Burton, W. K.; Cabrera, N.; Frank, F. C *Philos. Trans. R. Soc. London, Ser. A* **1951**, *243*, 299.
(71) Chernov, A. A.; Smol'skii, I. L.; Parvov V. F.; Kuznetsov, Yu. G.; Rozzhanskii, V. N. *Sov. Phys.-Crystallogr.* **1980**, *25*, 469.
(72) Durbin, S. D.; Feher, G. *J. Mol. Biol.* **1990**, *212*, 763.
(73) Durbin, S. D.; Carson, W. E. *J. Cryst. Growth* **1992,** *122*, 71.
(74) Durbin, S. D.; Carlson, W. E.; Saros, M. *J. Phys. D: Appl. Phys.* **1993**, *26*, B128.
(75) Konnert, J. H.; D'Antonio P.; Ward, K. B. *Acta Crystallogr., Sect. D* **1994,** *50*, 603.
(76) McPherson, A.; Malkin, A. J.; Kuznetsov, Yu. G. *Structure* **1995**, *3*, 759.
(77) Malkin, A. J.; Kuznetsov, Yu. G.; McPherson, A. *Proteins: Struct., Funct., Genet.* **1996**, *24*, 247.
(78) Malkin, A. J.; Kuznetsov, Yu. G.; McPherson, *J. Struct. Biol.* **1996**, *117*, 124.
(79) Malkin, A. J.; Kuznetsov, Yu. G.; Land, T. A.; DeYoreo, J. J.; McPherson, *Nat. Struct. Biol.* **1996**, *2*, 956.
(80) Malkin, A. J.; Kuznetsov, Yu. G.; Glantz, W.; McPherson, *J. Phys. Chem.* **1996**, *100*, 11736.
(81) Thiel, E. C. *Annu. Rev. Biochem.* **1987**, *56*, 289.
(82) Hempstead, P. D.; Yewdall, S. J.; Fernie, A. R.; Lawson, D. M.; Artymiuk, P. J.; Rice, D. W.; Ford, G. C.; Harrison, P. M. *J. Mol. Biol.* **1997**, *268*, 424.
(83) Yau, S.-T.; Vekilov, P. G. Manuscript in preparation.
(84) Thomas, B. R.; Carter, D.; Rosenberger, F. *J. Cryst. Growth* **1997**, *187*, 499.
(85) Chernov, A. A. *Annu. Rev. Mater. Sci.* **1973**, *3*, 397.
(86) Xiao, R.-F.; Alexander, J. I. D.; Rosenberger, F. *Phys. Rev. A* **1991**, *43*, 2977.
(87) Vekilov, P. G.; Rosenberger, F. *J. Cryst. Growth* **1996**, *158*, 540.
(88) Lin, H.; Rosenberger, F.; Alexander, J. I. D.; Nadarajah, A. *J. Cryst. Growth* **1995**, *151*, 153.
(89) Seeger, A. *Philos. Mag.* **1953**, *44*, 348.
(90) Wilcox, W. R. *J. Cryst. Growth* ***1977***, *37*, 229.
(91) Wilcox, W. R. *J. Cryst. Growth* **1983**, *65*, 133.
(92) Vekilov, P. G.; Monaco, L. A.; Rosenberger, F. *J. Cryst. Growth* **1995**, *156*, 267.
(93) Bauser E.; Strunk, H. *J. Cryst. Growth* **1981**, *51*, 362.
(94) Sherwood, J. N.; Shripathi, T. *J. Cryst. Growth* **1988**, *88*, 358.
(95) Sherwood, J. N.; Shripathi, T. *Faraday Discuss.* **1993**, *95*, 173.
(96) Frank, F. C. *J. Cryst. Growth* **1981**, *51*, 367.
(97) Gillig L. J.; Dam, B. *J. Cryst. Growth* **1984**, *67*, 400.
(98) General Discussion, *Faraday Discuss.* **1993**, *95*, 253.
(99) Chernov, A. A. *Modern Crystallography*; Springer: Berlin, 1984; Vol. III (Growth of Crystals), p 256.
(100) Kittel, C. *Introduction to Solid State Physics*, 6th ed.; Wiley: New York, 1986.
(101) Chernov, A. A.; Rashkovich, L. N.; Mkrtchan, A. A. *J. Cryst. Growth* **1986**, *74*, 101.
(102) Vekilov, P. G.; Kuznetsov, Yu. G. *J. Cryst. Growth* **1992**, *119*, 248.
(103) Meyers, M. C.; Chawla, K. K. *Mechanical Metallurgy*; Prentice Hall,: Eaglewood Cliffs, NJ, 1984; p 359.
(104) Cabrera, N.; Levine, M. *Philos. Mag.* **1956**, *1*, 450.
(105) van der Hoek, B.; van der Eerden, J. P.; Benema, P. *J. Cryst. Growth* **1982**, *56*, 621.
(106) Chernov, A. A.; Komatsu, H. In *Science and Technology of Crystal Growth*; van der Eerden, J. P., Bruinsma, O. S. L., Eds.; Kluwer: Amsterdam, 1995; p 67, 329.
(107) Nadarajah, A.; Pusey, M. L. *Acta Crystallogr., Sect. D* **1996**, *52*, 983.
(108) Nadarajah, A.; Pusey, M. L. *Acta Crystallogr., Sect. D* **1997**, *53*, 524.
(109) Li, M.; Nadarajah, A.; Pusey, M. L. *Acta Crystallogr., Sect. D* **1999**, *55*, 1036.
(110) Li, M.; Nadarajah, A.; Pusey, M. L. *Acta Crystallogr., Sect. D* **1999**, *55*, 1012.
(111) Forsythe, E. L.; Nadarajah, A.; Pusey, M. L. *Acta Crystallogr., Sect. D* **1999**, *55*, 1005.
(112) Kuznetsov, Y. G.; Malkin, A. J.; Land, T. A.; DeYoreo, J. J.; Barba, A. P.; Konnert, J.; McPherson, A. *Biophys. J.* **1997**, *72*, 2357−2364.
(113) Muschol, M.; Rosenberger, F. *J. Cryst. Growth* **1996**, *167*, 738.
(114) Sazaki, G.; Kurihara, K.; Nakada, T.; Miyashita, S.; Komatsu, H. *J. Cryst. Growth* **1996**, *169*, 355.
(115) Pusey, M.; Witherow, W.; Naumann, R. *J. Cryst. Growth* **1988,** *90*, 105.
(116) Miyashita, S.; Komatsu, H.; Suzuki, Y. *Jpn. J. Appl. Phys.* **1993,** *32*, 1855.
(117) Miyashita, S.; Komatsu, H.; Suzuki, Y.; Nakada, T. *J. Cryst. Growth* **1994,** *141*, 419.
(118) Land, T. A.; DeYoreo, J. J.; Lee, J. D. *Surface Sci.* **1997**, *384*, 136.
(119) Tanford, C. *Physical Chemistry of Macromolecules*; Wiley: New York, 1961.
(120) Cabrera, N.; Vermileya, D. A. In *Growth and Perfection of Crystals*; Doremus, R. H., Roberts, B. W., Turnbull, D., Eds.; Wiley: New York, 1958; p 393.
(121) Voronkov, V. V.; Rashkovich, L. N. *Soviet Phys., Crystallogr.* **1992**, *37*, 289.
(122) Voronkov, V. V.; Rashkovich, L. N. *J. Cryst. Growth* **1994**, *144*, 107.
(123) Vekilov, P. G.; Ataka, M.; Katsura, T. *Acta Crystallogr., Sect. D* **1995**, *51*, 207.
(124) Nakada, T.; Sazaki, G.; Miyashita, S.; Durbin, S. D.; Komatsu, H. *J. Cryst. Growth* **1999**, *196*, 503.
(125) Bliznakov, G. *Adsorption et Croissance Cristalline*; Centre National de la Recherche Scientifique: Paris, 1965; p 300. Bliznakov, G. *Fortsch. Min.* **1958**, *36*, 149.
(126) Chernov, A. A. *Modern Crystallography*; *Growth of Crystals*; Springer: Berlin, 1984; Vol. III, p 161.
(127) Chernov, A. A.; Parvov, V. F.; Kliya, M. O.; Kostomarov, D. V.; Kuznetsov, Yu. G. *Soviet Phys., Crystallogr.* **1981**, *26*, 640.
(128) Vekilov, P. G.; Kuznetsov, Yu. G.; Chernov, A. A *J. Cryst. Growth* **1992**, *121*, 643.
(129) Vekilov, P. G.; Kuznetsov, Yu. G.; Chernov, A. A *J. Cryst. Growth* **1992**, *121*, 44.
(130) Rashkovish, L. N.; Shekunov, B. Yu. *J. Cryst. Growth* **1990**, *100*, 133.
(131) Chernov, A. A. *Soviet Phys., Crystallogr.* **1972**, *16*, 734.
(132) Chernov, A. A. *J. Cryst. Growth* **1974**, *24/25*, 11.
(133) Chernov, A. A.; Malkin, A. J. *J. Cryst. Growth* **1988**, *92*, 432.
(134) Vekilov, P. G.; Kuznetsov, Yu. G.; Chernov, A. A *J. Cryst. Growth* **1990**, *102*, 706.
(135) Hirth, J.; Pound, G. *J. Chem. Phys.* **1957**, *26*, 1216.
(136) Gilmer, G. H.; Ghez, R.; Cabrera, N. *J. Cryst. Growth* **1971**, *8*, 79.
(137) Van der Eerden, J. P *J. Cryst. Growth* **1982**, *56*, 174.
(138) Chernov, A. A.; Corriel S. R.; Murray, B. T. *J. Cryst. Growth* **1993**, *132*, 405.
(139) Potapenko, S. Yu. *J. Cryst. Growth* **1996**, *158*, 346.
(140) Ehrlich, G.; Hudda, F. G. *J. Chem. Phys.* **1966**, *44*, 1039.
(141) Schwoebel, R. L.; Shipsey, E. J. *J. Appl. Phys.* **1966**, *37*, 3682.
(142) Autier, A, *J. Cryst. Growth* **1972**, *13/14*, 34.
(143) Fourme, R.; Ducruix, A.; Riess-Kautt, M.; Capelle, B. *J. Synchrotron Radiat.* **1995**, *2*, 136.
(144) Stojanoff, V.; Siddons, D. P.; Monaco, L. A.; Vekilov, P. G.; Rosenberger, F. *Acta Crystallogr., Sect. D* **1997**, *53*, 588.
(145) Izumi, K.; Sawamura, S.; Ataka, M. *J. Cryst. Growth* **1996**, *168*, 106.
(146) Otalora, F.; Garcia-Ruiz, J.-M. *J. Cryst. Growth* **1998**, *196*, 546.
(147) Vidal, O. *J. Cryst. Growth* **1998**, *196*, 559

(148) Vekilov, P. G.; Monaco, L. A.; Thomas, B. R.; Stojanoff, V.; Rosenberger, F. *Acta Crystallogr., Sect. D* **1996**, *52*, 785.
(149) Caylor, C. L.; Dobrianov, I.; Kimmer, C.; Zipfel, W.; Thorne, R. E. *Phys. Rev. E* **1999**, *59*, R3831.
(150) Weisgerber, S.; Helliwell, J. R. *Acta Crystallogr., Sect. D* **1995**, *51*, 1099.
(151) Snell, E.; Cassetta, A.; Helliwell, J. R.; Boggon, T. J.; Chayen, N. E.; Weckert, E.; Hölzer, K.; Schroer, K.; Gordon, E. J.; Zagalski, P. F. *Acta Crystallogr., Sect. D* **1997**, *53*, 231.
(152) Guinier, A *Cryst. Res. Technol.* **1998**, *33*, 543.
(153) Braun, N.; Tack, J.; Weinkauf, S. *7th International Conference on Crystallization of Biological Macromolecules*, Granada, Spain, May 3−8, 1998.
(154) Weinkauf, S.; Bachmann, L. *Ultramicroscopy* **1992**, *46*, 113.
(155) Bachmann, L.; Weinkauf, S.; Baumeister, W.; R.; Bacher, A *J. Mol. Biol.* **1989**, *207*, 575.
(156) Weinkauf, S.; Bacher, A.; Baumeister, W.; Ladenstein, R.; Huber, R.; Bachmann, L. *J. Mol. Biol.* **1991**, *221*, 637.
(157) Püler, G.; Weinkauf, S.; Bachmann, L.; Müler, S.; Engel, A.; Hegerl, R.; Baumeister, W. *EMBO J.* **1992**, *11*, 1607.
(158) Meining, W.; Bacher, A.; Bachmann, L.; Schmid, C.; Weinkauf, S.; Huber, R.; Nar, H. *J. Mol. Biol.* **1995**, *253*, 208.
(159) Rübenkamm, E.; Braun, N.; Bachmann, L.; Bacher, A.; Brandt, J.; Baumeister, W.; Weinkauf, S. *Ultramicroscopy* **1995**, *58*, 337.
(160) Braun, N.; Tack, J.; Bachmann, L.; Weinkauf, S. *Thin Solid Films* **1996**, *284−285*, 703.
(161) Bacher, A.; Weinkauf, S.; Bachmann, L.; Ritser, K.; Baumeister, W.; Huber, R.; Ladenstein, R. *J. Mol. Biol.* **1992**, *225*, 1065.
(162) Weinkauf, S. Technical University Munich, 1998, private communication.
(163) Vekilov, P. G.; Alexander, J. I. D.; Rosenberger, F. *Phys. Rev. E* **1996**, *54*, 6650.
(164) Onuma, K.; Kameyama, T.; Tsukamoto, K. *J. Cryst. Growth* **1994**, *137*, 610.
(165) Ristic, R. I.; Shekunov, B.; Sherwood, J. N. *J. Cryst. Growth* **1996**, *160*, 330.
(166) Shekunov, B. Yu.; Rashkovich, L. N.; Smol'skii, I. L. *J. Cryst. Growth* **1992**, *116*, 340.
(167) Lin, H.; Vekilov P. G.; Rosenberger, F. *J. Cryst. Growth* **1996**, *158*, 552.
(168) Bauser, E. In *Handbook of Crystal Growth*; Hurle, D., Ed.; Amsterdam: North-Holland, 1994; Vol. 3b, p 879.
(169) Vekilov, P. G.; Rosenberger, F. *Phys. Rev. E* **1998**, *57*, 6979.
(170) Monaco, L. A.; Rosenberger, F. *J. Cryst. Growth* **1993**, *129*, 465.
(171) Chernov, A. A. *Modern Crystallography III: Growth of Crystals*; Springer: Berlin, 1984; p 247.
(172) Potapenko, S. Yu. *Physica A* **1996**, *230*, 631
(173) Potapenko, S. Yu. *J. Cryst. Growth* **1996**, *158*, 346.
(174) Wilcox, W. R. *J. Cryst. Growth* **1977**, *38*, 73.
(175) Haase, C. S.; Chadam, J.; Feinn, D.; Ortoleva, P. *Science* **1980**, *209*, 272.
(176) Ortoleva, P. J. *Geochemical Self−Organization*; University Press: Oxford, **1994**.
(177) Allegre, C. J.; Provost, A.; Jaupart, C. *Nature* **1981**, *294*, 223.
(178) Favier, J. J. *J. Electrochem. Soc.* **1982**, *129*, 2355.
(179) Koper, M. *Far-From-Equilibrium Phenomena in Electrochemical Systems. Instabilities, Oscillations and Chaos*; University of Utrecht Press: Utrecht, 1994.
(180) Garcia-Ruiz, J. M.; Rondon, D.; Garcia-Romero, A.; Otalora, F. *J. Phys. Chem.* **1996**, *100*, 8854.
(181) Garcia-Ruiz, J. M.; Santos, A.; Alfaro, E. J. *J. Cryst. Growth* **1987**, *84*, 555.
(182) Cross M. C.; Hohenberg, P. C. *Rev. Mod. Phys.* **1993,** *65*, 851.
(183) Gray, P.; Scott, S. K. *Chemical Oscillations and Instabilities. Nonlinear Chemical Kinetics*; Clarendon Press: Oxford, 1990.
(184) Chernov, A. A. *Modern Crystallography*; Springer: Berlin, 1984; Vol. III (Growth of Crystals), p 208.
(185) Vekilov, P. G.; Lin, H.; Rosenberger, F. *Phys. Rev. E* **1997,** *55*, 3202.
(186) Frank, F. C. In *Growth and Perfection of Crystals*; Doremus, R. H., Roberts, B. W., Turnbull, D., Eds.; Chapman and Hill: London, 1958; p 411.
(187) Lighthill, M. J.; Whitham, G. B. *Proc. R. Soc. A* **1955**, *229*, 317.
(188) Helbing, D.; Treiber, M. *Science* **1998**, *282*, 2001. Helbing, D.; Treiber, M. *Phys. Rev. Lett.* **1998**, *81*, 3042.
(189) Lee, H. Y.; Lee, H.-W.; Kim, D. *Phys. Rev. Lett.* **1998**, *81*, 1130.
(190) Sunagawa, I. In *Materials Science of the Earth's Interior*; Sunagawa, I., Ed.; Terra: Tokyo, 1984; pp 303, 323.
(191) Sunagawa, I.; Bennema, P. *J. Cryst. Growth* **1979,** *46*, 451.
(192) van Leeuven, C.; van Rosmalen, R.; Bennema, P. *Surf. Sci.* **1974**, *44*, 213.
(193) Uwaha, M.; Saito, Y.; Sato, M. *J. Cryst. Growth* 1995, *146*, 164.
(194) Saito, Y.; Uwaha, M. *Phys. Rev. B* **1995**, *51*, 11172.
(195) Chernov, A. A.; Kuznetsov, Yu. G.; Smol'skii, I. L.; Rozhanskii, V. N. *Sov. Phys., Crystallogr.* **1986**, *31*, 705.
(196) Chernov, A. A. *J. Cryst. Growth* **1992**, *118*, 333.
(197) Potapenko, S. Yu. *J. Cryst. Growth* **1995** *147*, 223.
(198) Coriell, S. R.; Chernov, A. A.; Murray, B. T.; McFadden, G. B. *J. Cryst.Growth* **1998,** *183*, 669.
(199) Yoo, H. D.; Wilcox, W. R.; Lal, R. B.; Trolinger, J. D. *J. Cryst. Growth* **1988,** *92*, 101.
(200) Onuma, K.; Tsukamoto, T.; Sunagawa, I. *J. Cryst. Growth* **1988**, *89*, 177.
(201) Coriell, S. Private communication.
(202) Chernov, A. A. *Soviet Phys., Uspekhi* **1961,** *4*, 116.
(203) Williams, E. D.; Bartelt, N. C. *Science* **1991**, *251*, 393;
(204) Bartelt, N. C.; Einstein; T. L.; Williams, E. D. *Surf. Sci. Lett.* **1990**, *240*, L591.
(205) Rosenberger, F.; Lin, H.; Vekilov, P. G. *Phys. Rev. E* **1999**, *59*, 3155.
(206) Vekilov, P. G.; Rosenberger, F.; Lin, H.; Thomas, B. R. *J. Cryst. Growth* **1999**, *196*, 261.
(207) Maiwa, K.; Plomp, M.; van Enckevort, W. J. P.; Bennema, P. *J. Cryst. Growth* **1998**, *186*, 214.
(208) Lafont, S.; Veesler, S.; Astier, J. P.; Boistelle, R. *J. Cryst. Growth* **1997**, *173*, 132.
(209) Provost, K.; Robert, M. C. *J. Cryst. Growth* **1995**, *156*, 112.
(210) Garcia Ruiz, J. M.; Moreno, A. *Acta Crystallogr., Sect. D* **1995**, *51*, 278.
(211) Levich, V. G. *Physicochemical Hydrodynamics*; Prentice Hall: Englewood Cliffs, 1962.
(212) Schlichting, H. *Boundary Layer Theory*, 6th ed.; McGraw-Hill: New York, 1968.
(213) Durbin, S. D.; Feher, G. *J. Cryst. Growth* **1986**, *76*, 583
(214) Nyce, T. A.; Rosenberger, F. *J. Cryst. Growth* **1991**, *110*, 52.
(215) Grant, M. L.; Saville, D. A. *J. Cryst. Growth* **1995**, *153*, 42.
(216) Littke, W.; John, Chr. *Science***1984**, *225*, 203. Littke, W.; John, Chr. *J. Cryst. Growth* **1986**, *76*, 663.
(217) Day, J.; McPherson, A. *Protein Sci.* **1992**, *1*, 1254.
(218) DeLucas, L. J.; *J. Cryst. Growth* **1994**, *135*, 183.
(219) Durbin, S. D.; Feher, G. *Annu. Rev. Phys. Chem.* **1996**, *47*, 171.
(220) Grant, M. L.; Saville, D. A. *J. Cryst. Growth* **1991**, *108*, 8
(221) Vekilov, P. G.; Rosenberger, F. *J. Cryst. Growth* **1998**, *186*, 251.
(222) Fredericks, W. J.; Hammond, M. C.; Howard, S. B.; Rosenberger,. F. *J. Cryst. Growth* **1994**, *141*, 183.
(223) Vekilov, P. G.; Rosenberger, F. *Phys. Rev. Lett.* **1998**, *80*, 2654.
(224) Vekilov, P. G.; Thomas, B. R; Rosenberger, F. *J. Phys. Chem.* **1998**, *102*, 5208.
(225) Malkin, A. J.; Kuznetsov, Yu. G.; McPherson, A. *Surf. Sci.* **1997**, *393*, 95.
(226) Kuznetsov, Yu. G.; Malkin, A. J.; McPherson, A. *Phys. Rev. B* **1998**, *58*, 6097.
(227) McPherson, A. *J. Phys. D*: *Appl. Phys.* **1993**, *26*, 104.
(228) McPherson, A. In *Proceedings of the Eighth European Symposium on Materials and Fluid Science in Microgravity;* ESA SP-333: Brussels,1992; p 619.
(229) Thomas, B. R.; Vekilov, P. G.; Rosenberger, F. *Acta Crystallogr., Sect. D* **1998,** *54*, 226.
(230) DeLucas, L. J.; Sudath, F. L.; Snyder, R.; Naumann, R.; Broom, M. B.; Pusey, M.; Yost, V.; Herren, B.; Carter, D.; Nelson, B.; Meehan, E. J.; McPherson, A.; Bugg. C. E *J. Cryst. Growth* **1986**, *76*, 681.
(231) Hilgenfeld, R.; Liesum, A.; Storm, R.; Plaas-Link, A. *J. Cryst. Growth* **330** , *122*, 1992.
(232) Broutin, I.; Ries-Kautt, M.; Ducruix, A. *J. Cryst. Growth* **1997**, *181*, 97.
(233) Kadima, W.; McPherson, A.; Dunn, M. F.; Jurnak, F. *Biophys. J.* **1990**, *57*, 125.
(234) Rosenberger, F., Vekilov, P. G., Lin, H.; Alexander, J. I. D. *Microgravity Sci. Technol.* **1997**, *10*, 29.
(235) Snell, E. H.; Weisgerber, S.; Helliwell, J. R.; Weckert, F.; Hölzer, K.; Schroer, K. *Acta Crystallogr., Sect. D* **1995,** *51*, 1099.
(236) Ng, J. D.; Lorber, B.; Giege, R.; Koszelak, S.; Day, J.; Greenwood, A.; McPherson, A. *Acta Crystallogr., Sect. D* **1997**, *53*, 724.
(237) Carter, D. C.; Ho, J. X.; Wright, B. S.; Twigg, P. D.; Miller, T. Y.; Chapman, J.; Keeling, K.; Ruble, J.; Lim, K.; Vekilov, P. G.; Thomas, B. R.; Chernov, A. A. *J. Cryst. Growth* **1998**, *196*, 623.
(238) Vekilov, P. G.; Alexander, J. I. D. Manuscript in preparation.
(239) Rashkovich, L. N. *KDP−Family of Crystals*; Adam Hilger: Bristol, 1991.
(240) Chernov, A. A. *Z. Phys. Chemie Leipzig* **1988**, *269*, 941. Chernov, A. A. *Contemp. Phys.* **1989**, *30*, 251.
(241) Görnert, P.; Voigt, F. In *Current Topics in Materials Science*; Kaldis, E., Ed.; North-Holland: Amsterdam, 1984; p 1.
(242) van der Eerden, J. P.; Müller-Krumbhaar, H. *Phys. Rev. Lett.* **1986**, *57*, 2431. van der Eerden, J. P.; Müller-Krumbhaar, H. *Electrochim. Acta* **1986**, *31*, 1007.
(243) van Enckevort, W. J. P. *Prog. Cryst. Growth Charact.* **1984**, *9*, 1.
(244) Rashkovich, L. N.; Kronsky, N. V. *J. Cryst. Growth* **1997**, *182*, 434.
(245) Fleury, V. *Nature* **1997**, *390*, 145.
(246) Vinson, M.; Mironov, S.; Mulvey, S.; Pertsov, A. *Nature* **1997**, *386*, 477.
(247) Witkowski, F. X.; Leon, L. J.; Penkoske, P. A.; Giles, W. R.; Spano, M. L.; Ditto, W. L.; Winfree, A. T. *Nature* **1998**, *392*, 78.

CR9800558